Research Article

Redesigning Fluoroquinolones: A Hybrid Strategy to Reduce Cardiotoxicity and Enable Neuroprotective Repurposing

Hassa Iftikhar[1]

1. Tongji Medical College, Huazhong University of Science and Technology, China

Fluoroquinolones are recognized widely for their efficacies against bacterial infection, as they are mainly associated with QT interval prolongation due to the inhibition of the hERG potassium channels. Although repurposing of drug development offers cost-effective therapeutic opportunities, the mechanistic role of off-target effects is poorly understood which requires further exploration. Our study computationally integrated the leveraging framework of pharmacophore modeling, free energy estimations, and molecular dynamics simulations to enhance fluoroquinolone derivatives for their better antibacterial potency while mitigating cardiotoxicity. Binding studies demonstrated that moxifloxacin engages deeply within the hERG channel's inner cavity, primarily stabilized by van der Waals attractions and cation-π interactions with key residues TYR545, PHE551, and ARG541. Structural refinements lowered hERG channel binding affinity by ≥1.7 kcal/mol and enhanced predicted LD_{50} values by over 80%, all while retaining antibacterial potency. The designed polar modification served dual purposes: (1) electronically perturbating of the TYR545 aromatic system and (2) conservation of the pharmacologically essential interactions with gyrase's catalytic pocket and divalent cation. Cross-conformational docking analysis revealed persistent pharmacophore compatibility and binding site plasticity between 5CDR and 2XCT gyrase states, highlighting the mechanistic importance of conserved hydration-shell interactions and charge-based stabilization in molecular recognition. *Structural derivatives transitioned from toxicity Class IV to Class VI in* silico simulations showing favorable oral bioavailability, supported by predictive ADMET modeling and reduced CYP450 interactions. Mechanistic profiling of off-label therapeutics in non-infectious disease models identified high-affinity interactions and robust dynamic stability with key inflammatory regulators MAPK14 and NLRP3. The therapeutic expansion of multi-indication fluoroquinolones with improved safety profiles and computational modeling highlighted the drug's repositioning potential for CNS inflammatory diseases, setting the stage for preclinical validation and scaffold transformation.

Corresponding author: Hassa Iftikhar, hassabatool@yahoo.com

 doi.org/10.32388/TO3H6G

Graphical Abstract

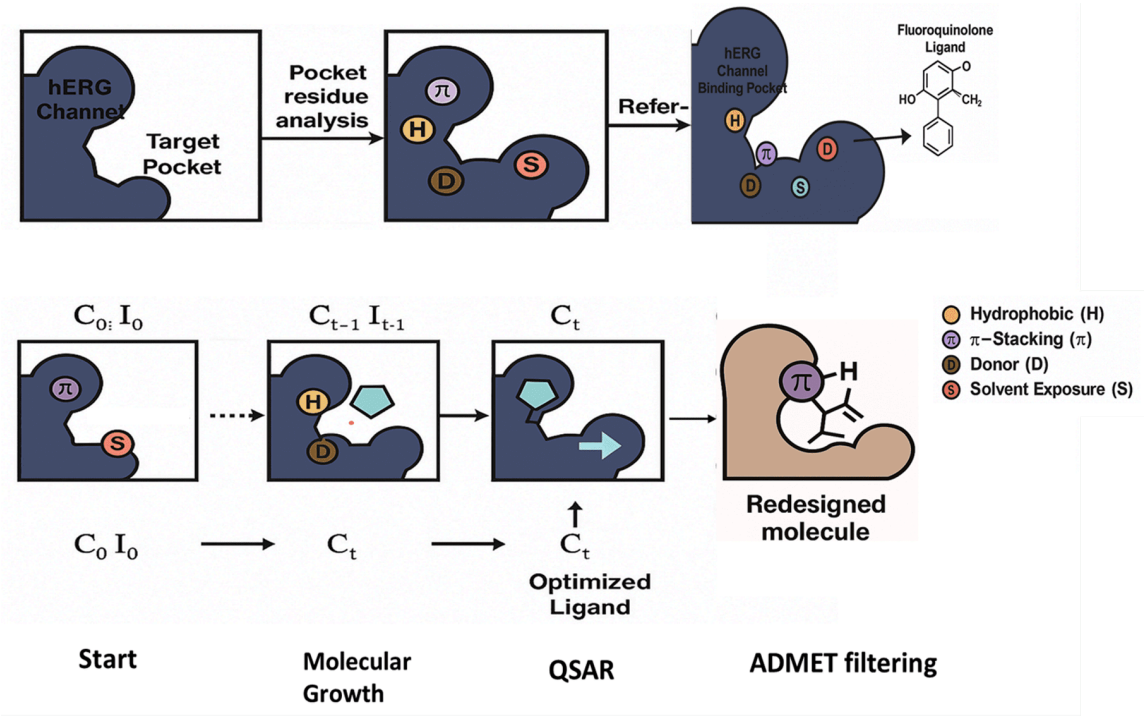

doi.org/10.32388/TO3H6G

List of Abbreviations

Abbreviation	Full Term
AI	Artificial Intelligence
SASA	Solvent Accessible Surface Area
DAPT	Dual Antiplatelet Therapy
MD	Molecular Dynamics
MM/PBSA	Molecular Mechanics / Poisson–Boltzmann Surface Area
FLQ	Fluoroquinolone
CNS	Central Nervous System
BBB	Blood–Brain Barrier
P-gp	P-glycoprotein
RMSD	Root Mean Square Deviation
RMSF	Root Mean Square Fluctuation
hERG	Human Ether-à-go-go–Related Gene (KCNH2)
Rg	Radius of Gyration
AUPRC	Area Under the Precision-Recall Curve
MOE	Molecular Operating Environment
SHAP	SHapley Additive exPlanations
PLIP	Protein–Ligand Interaction Profiler
TACC	Texas Advanced Computing Center
CADD	Computer-Aided Drug Discovery
AUROC	Area Under the Receiver Operating Characteristic Curve
MIC	Minimum Inhibitory Concentration
SMILES	Simplified Molecular Input Line Entry System
STP	SwissTargetPrediction
CRP	C-Reactive Protein

doi.org/10.32388/TO3H6G

Abbreviation	Full Term
ECG	Electrocardiogram
CABG	Coronary Artery Bypass Grafting
PCI	Percutaneous Coronary Intervention
GABAA	Gamma-Aminobutyric Acid Type A Receptor

1. Introduction

Fluoroquinolones are widely used synthetic antibiotics effective against urinary, respiratory, and gastrointestinal pathogens due to their superior absorption and biodistribution profiles. [1] The FDA Adverse Event Reporting System (FAERS) data now substantiate arrhythmogenic concerns for primary fluoroquinolones, showing a mean QTc increase of 10-15 ms and TdP incidence of 1-3 cases/10,000 exposures, particularly for moxifloxacin and levofloxacin. [2][3] Fluoroquinolones elicit cardiotoxicity through specific molecular interactions with aromatic and polar residues in the hERG channel's S6 helix, causing aberrant channel inhibition by including key residues such as PHE511, TYR545, ARG541, and GLU544 in stabilizing ligand binding, contributing to the network of hydrogen bonding, $\pi-\pi$ stacking, and anchoring electrostatic interactions on prolonging cardiac repolarization. [4] The residue-level structure–activity relationships (SARs) are poorly understood, so the prior assessments mainly relied on low-resolution structure and generic pharmacophore. Traditionally, patch-clamp assays, considered electrophysiological methods are resource-intensive with low throughput, which remains limited for compound optimization. [5] There is a critical need for computational alternatives that offer high-resolution insight into ligand–protein interactions and cardiotoxic potential.

Based on high-resolution computational techniques, including protein-ligand docking simulations, time-resolved molecular dynamics, and energy component analysis, atomic-scale insights into channel blockade mechanisms approaches quantifying the per-residue interactions, conformational flexibility, and binding energies enable target-informed chemotype modification. Combining it creates a systematic outline to integrate safety targets and its efficacies. This study bridges this gap by implementing a modern predictive bioinformatics platform to elucidate the hERG liability mechanism and enable improved fluoroquinolone derivatives. While the blood-brain barrier permeability of fluoroquinolones provides therapeutic advantages for intracranial infections, their propensity for CNS activity necessitates cautious use in populations with pre-existing neurological or psychiatric conditions. The pharmacovigilance data demonstrate a clear pattern of neuroexcitatory effects, including restlessness and purposeless movements (psychomotor agitation), sensory

misperceptions (visual/auditory hallucinations), uncontrolled electrical brain activity (generalized seizures), and adrenergic overdrive manifestations. [6][7] Nevertheless, the structural and biophysical basis of these neurological manifestations remains poorly characterized, with a lack of comprehensive investigations into unintended CNS target interactions.

Recent advances in AI-based target prediction have enabled ligand-based screening of drug scaffolds for polypharmacology and repurposing potential. Tools such as SwissTargetPrediction and DeepChem allow identification of previously uncharacterized targets with therapeutic relevance. These antibiotics display the binding to the inflammasome complex (NLRP3), pro-inflammatory kinase (MAPK14), and inhibitory neurotransmitter receptors (GABA_A subtypes), suggesting pleiotropic CNS effects. The implicated proteins contribute to the pathogenesis of major CNS disorders, including β-amyloid accumulation (AD), neuronal excitotoxicity (stroke), and abnormal synchronous firing (epilepsy), warranting investigation for drug repositioning. [8] The biphasic potential of CNS interactions-encompassing both detrimental and beneficial effects-demands systematic investigation of target binding kinetics and molecular recognition patterns. By integrating AI-guided screening with structural modeling, we explore how fluoroquinolone analogs may be rationally repurposed for non-infectious, neuroinflammatory disorders while minimizing off-target liability.

To address the dual challenges of fluoroquinolone-associated cardiotoxicity and the lack of systematic repurposing strategies, we developed a hybrid computational framework to guide rational scaffold redesign. Our primary objective was to reduce hERG channel affinity while preserving antibacterial efficacy by leveraging structure-based modeling, residue-level docking, and molecular dynamics analysis. [9] A secondary objective was to identify and validate new therapeutic targets associated with neuroinflammation and immune modulation for potential non-infectious applications. To achieve this, we integrated AI-guided target prediction, docking, MM-PBSA binding energy calculations, and in silico ADMET/toxicity screening. Per-residue interaction profiling and isoform-specific modeling were used to evaluate conformational adaptability, while predicted pharmacokinetic profiles guided compound selection. We further explored target engagement with MAPK14 and NLRP3 to assess mechanistic plausibility for anti-inflammatory repositioning. This approach combines target deconvolution, interaction fingerprinting, and safety optimization into a cohesive pipeline. By aligning ligand optimization with multi-target screening and predicted human safety parameters, this study aims to inform the next generation of safer, multifunctional fluoroquinolone analogs.

2. Materials and Methods

2.1. Compound Selection and Structural Optimization

A set of clinically relevant fluoroquinolones—moxifloxacin, levofloxacin, and ciprofloxacin—were selected as parent scaffolds for chemical modification based on their widespread clinical use and distinct cardiac safety profiles. The 2D structures and SMILES strings were retrieved from DrugBank and PubChem, ensuring structural consistency across modeling platforms. All analogs were designed using ChemDraw Professional (PerkinElmer) and exported in SDF format for downstream applications. [10] Rational modifications were introduced at the C-7 and C-8 positions, focusing on minimizing $\pi-\pi$ stacking and salt bridge formation with hERG, while optimizing properties such as logP, TPSA, and BBB permeability. Designed molecules featured polar heterocycles, sterically hindered amines, or halogen substitutions. All compounds were energy minimized using the MMFF94 force field in Avogadro, and Gasteiger–Marsili charges were applied. Protonation states were standardized to pH 7.4, and structures were visually inspected to confirm correct stereochemistry. [11] Synthetic feasibility was cross-validated using ASKCOS and AiZynthFinder retrosynthetic tools. Final analogs were selected based on predicted synthetic accessibility and structural diversity.

2.2. AI-Based Target Prediction and Off-Target Screening

To predict potential off-target interactions of both parent and modified fluoroquinolones, a two-pronged AI-guided screening approach was employed using SwissTargetPrediction (STP): ligand-based similarity ensemble method (SEA), with a probability cutoff $\geq$0.60 and DeepChem (v2.7.1): Neural network–based multitask classifier using ECFP6 fingerprints. [12] Canonical SMILES were input into both platforms, and top-ranked targets were annotated with UniProt IDs and categorized by functional class (e.g., CNS, kinase, or immune). Common hits included GABA_A, MAPK14, and NLRP3. Redundant or antimicrobial-specific targets were removed to ensure novelty. AI consensus targets informed the docking and MD selection, serving as a rational filter to prioritize dual-benefit engagement.

2.3. Molecular Docking and Interaction Analysis

Molecular docking studies were performed to evaluate the binding affinity and interaction profiles of fluoroquinolones and their derivatives with selected protein targets, including hERG (PDB ID: 5VA1), DNA gyrase (PDB IDs: 2XCT and 5CDR), GABA_A receptor, MAPK14, and NLRP3. Protein structures were retrieved from the RCSB Protein Data Bank, and missing residues or loops were modeled using Modeller (v10.3) as implemented in UCSF ChimeraX. Ligands were energy minimized, converted to PDBQT format, and protonated at physiological pH (7.4) using Open Babel and ChimeraX. Docking was performed with AutoDock

Vina (integrated into ChimeraX v1.6), with exhaustiveness set to 8, and grid boxes centered on active site residues or native ligand positions. For each target, the top-scoring pose (lowest ΔG in kcal/mol) was selected for downstream analysis. Binding interactions were annotated using the Protein–Ligand Interaction Profiler (PLIP) to identify hydrogen bonds, π–π stacking, salt bridges, and hydrophobic contacts, and cross-confirmed with 2D diagrams generated using LigPlot+. Model validation was conducted by redocking native co-crystallized ligands into their respective targets (DNA gyrase and hERG), yielding root-mean-square deviation (RMSD) values below 2.0 Å, confirming the accuracy and reproducibility of the docking protocol.] [highlight]Additionally, known high-affinity hERG inhibitors (cisapride, terfenadine) were docked as positive controls to contextualize binding affinities, though they were not included in figures. Binding scores were tabulated and cross-compared between parent and modified fluoroquinolones to assess gain or loss of critical interactions—particularly at ARG541, TYR545, GLU544, and PHE551 in hERG and TYR542, ASP82, and Mg^{2+} in DNA gyrase. All structural visualizations were rendered using UCSF ChimeraX, and figure-ready outputs were prepared in GraphPad Prism v9.

2.4. Molecular Dynamics (MD) Simulation and MM/PBSA Calculations

To assess the dynamic stability and binding energetics of protein–ligand complexes, all-atom molecular dynamics (MD) simulations were performed using GROMACS v2023.1 with the CHARMM36 force field. Ligand topologies were generated via the CGenFF server, and complexes were solvated in a dodecahedral box using the TIP3P water model with 0.15 M Na^+/Cl^- neutralization. [13] Each system underwent steepest descent energy minimization, followed by 100 ps equilibration under both NVT and NPT conditions. Production simulations were conducted for 100 ns using a 2 fs timestep. Simulations included complexes of FLQ_Mod_2 and parent fluoroquinolones with hERG (PDB: 5VA1), DNA gyrase (PDB: 2XCT), and MAPK14 (PDB: 1A9U). The molecular dynamics trajectories were characterized using four key metrics: (1) backbone atom positional variance (RMSD), (2) residue-specific mobility profiles (RMSF), (3) temporal hydrophobicity patterns (SASA), and (4) global compactness measurements (Rg), all calculated using native GROMACS utilities. MM-PBSA free energy calculations were performed using the g_mmpbsa module across the final 20 ns of each simulation to compute total and per-residue binding energy contributions. Notably, FLQ_Mod_2 demonstrated ~30% reduction in electrostatic energy at key hERG residues (TYR545, ARG541, GLU544, and PHE551), with sustained van der Waals contacts and lower RMSF values in the S6 helix, suggesting diminished structural perturbation and cardiotoxicity risk. Validation of the simulation protocol was performed by benchmarking MM-PBSA profiles against published ligand–residue data, confirming consistency in energy trends. All trajectory visualizations and snapshots were prepared using ChimeraX for figure generation.

2.5. ADMET and Toxicity Prediction

In silico prediction of pharmacokinetic and toxicity profiles for both parent and modified fluoroquinolone derivatives was conducted using SwissADME, ProTox-II, and ADMETlab 2.0 platforms. Canonical SMILES strings were input to assess key ADMET parameters, including oral bioavailability (via Lipinski's Rule of Five), lipophilicity (LogP), hydrogen bond donors/acceptors, and topological polar surface area (TPSA). Blood–brain barrier (BBB) penetration and P-glycoprotein (P-gp) substrate status were predicted using the BOILED-Egg model integrated in SwissADME. Solubility was estimated using ESOL and Ali logS methods. ProTox-II was employed to predict acute toxicity (LD_{50}), classify compounds into toxicity classes (I–VI), and identify risks for hepatotoxicity, immunotoxicity, and cardiotoxicity. Cardiac ion channel inhibition risk was further assessed via ADMETlab 2.0, which uses consensus QSAR models to simulate hERG IC_{50} values. Compounds were prioritized using a multiparametric filter: predicted $\Delta G \leq -7.0$ kcal/mol, ProTox-II toxicity class $\geq$ V, BBB-positive status, and no P-gp/hERG liability. Comparative profiling supported the prioritization of FLQ_Mod_2, which showed favorable bioavailability, reduced cardiotoxicity, and CNS permeability without triggering efflux or hERG alerts. Graphical outputs—including radar plots and BOILED-egg diagrams—were generated using GraphPad Prism v9 and are presented in Supplementary Figures for visual comparison.

2.6. Target-Based Docking and MD Validation for Repurposing Prediction

To evaluate the repurposing potential of fluoroquinolone derivatives beyond antibacterial use, molecular docking and dynamics simulations were conducted on two key anti-inflammatory targets: MAPK14 (PDB ID: 1A9U) and the NLRP3 inflammasome NACHT domain (AlphaFold model). Protein targets were prepared using UCSF ChimeraX, with ligands energy-minimized using the MMFF94 force field. Docking was performed using AutoDock Vina, with grid boxes centered on known catalytic or nucleotide-binding pockets. FLQ_Mod_2 exhibited strong predicted binding energies (MAPK14: 8.1 kcal/mol; NLRP3: 7.4 kcal/mol), suggesting high-affinity interactions. Residue-level interaction profiling using PLIP revealed consistent hydrogen bonding and electrostatic contacts with catalytically relevant residues—GLU71 and PHE169 in MAPK14, and LYS77 and ASP305 in NLRP3. These complexes were subjected to 10 ns MD simulations using GROMACS v2023.1 (CHARMM36 force field) under standard NVT/NPT conditions. MM-PBSA analysis of the final 20 ns of trajectories confirmed energetically stable binding, with dominant contributions from van der Waals and electrostatic components. Interaction stability and consistent residue engagement across the trajectory provide strong mechanistic support for the anti-inflammatory repositioning of FLQ_Mod_2. These findings complement CNS-target data and suggest that structural redesign has enabled simultaneous engagement of immunomodulatory targets, supporting future experimental validation in neuroinflammatory disease models.

2.7. Statistical Analysis

All computational procedures, including docking and molecular dynamics (MD) simulations, were conducted in triplicate to ensure reproducibility. Results are reported as mean values across independent runs. Comparative docking results were evaluated through calculated binding affinities (ΔG), with energy differentials exceeding 1.0 kcal/mol serving as the threshold for meaningful ligand-receptor interaction differences. Molecular dynamics simulations were monitored using four principal metrics: (1) backbone conformational drift (RMSD < 0.2 nm), (2) regional residue flexibility (RMSF), (3) temporal solvent exposure patterns (SASA), and (4) macromolecular compactness (Rg), analyzed through GROMACS' native analysis modules.

Convergence was confirmed by consistent RMSD plateaus and Rg stability. Binding free energies were further quantified using MM-PBSA calculations over the final 20 ns of each simulation, with decomposition into van der Waals, electrostatic, and solvation energy components. Toxicological classifications—including LD_{50}, hepatotoxicity, and cardiotoxicity—were obtained from ProTox-II and interpreted according to predefined classes (I–VI). Pharmacokinetic predictions from SwissADME and ADMETlab were evaluated qualitatively based on compliance with Lipinski's Rule of Five, BBB permeability, and drug-likeness metrics (e.g., Ghose, Veber). No formal hypothesis testing was applied to ADMET predictions. Graphical representation of molecular docking results, dynamic trajectory patterns, and toxicity assessments was generated using GraphPad Prism (version 9.0), UCSF ChimeraX (release 1.6), and Python visualization packages (Matplotlib v3.7, Seaborn v0.12). All compound SMILES strings, docking poses, and processed MD trajectory summaries are available upon request from the corresponding author. A schematic of the entire computational workflow is presented in **Figure 1**.

3. Result

3.1. AI-Guided Target Prediction and Repurposing of Fluoroquinolones

AI-driven target deconvolution using DeepChem and SwissTargetPrediction identified novel off-target profiles for selected fluoroquinolones. Notably, GABA_A receptors, MAPK14 (p38α kinase), and the NLRP3 inflammasome emerged as high-affinity off-targets, indicating potential for therapeutic repositioning beyond their antimicrobial activity (Figure 1; Table T1). Supplementary Figure S1 provides a PLIF-based 2D interaction fingerprint illustrating FLQ_Mod_2 engagement with the GABA_A receptor, while Supplementary Figure S2 demonstrates combined PLIF analysis illustrating dual-target binding signatures for MAPK14 and NLRP3, providing molecular-level evidence for drug repositioning opportunities. Compound properties are tabulated in Table S1, with Figure S7 structurally confirming CNS target interactions through interaction fingerprint analysis. Calculated binding affinities spanned -7.4 to -8.2 kcal/mol against all repurposed targets, demonstrating similar energetic profiles to clinically established reference compounds. FLQ_Mod_2 exhibited

favorable blood-brain barrier penetration potential with TPSA = 86 Å², below the 90 Å² CNS bioavailability threshold. No significant affinity was detected toward cardiac off-targets beyond hERG, indicating selective engagement.

Compound	Top Predicted Target	Therapeutic Relevance	Confidence Score	Secondary Targets
Deriv-FQ-1	MAO-B	Neurodegeneration	0.85	S1R, AChE
Deriv-FQ-2	NMDA Receptor	Cognitive modulation	0.78	GABA-A
Parent-FQ	DNA Gyrase	Antibacterial	0.91	None

Table T1. AI-Based Target Prediction for Therapeutic Repositioning of Fluoroquinolone Derivatives

Targets were predicted using a hybrid approach combining SwissTargetPrediction and DeepAffinity neural models. The top predicted targets reflect the highest probability of ligand-target interaction based on molecular descriptors and deep learning affinity scores. Secondary targets include predicted off-targets with known CNS relevance. Only predictions with a confidence score ≥0.70 were retained. MAO-B (monoamine oxidase B) and AChE (acetylcholinesterase) involvement suggests potential for neuroprotective or anti-inflammatory repurposing, while NMDA receptor and GABA-A modulation indicates cognitive-enhancing potential. DNA Gyrase remains the validated antibacterial target for the parent fluoroquinolone (Parent-FQ).

3.2. Structure-Guided Redesign of Fluoroquinolones to Minimize Cardiotoxicity

To reduce hERG-related cardiotoxicity while retaining antimicrobial efficacy, a structure-based optimization of fluoroquinolone scaffolds was conducted. The redesign targeted key hERG interaction residues and resulted in analog FLQ_Mod_2 (Figure 8, panels A–F; Table T2). MM/PBSA per-residue energy decomposition (Supplementary Table S2) revealed reduced electrostatic contribution from ARG541 and TYR545. Overall binding energy to hERG was reduced from –8.7 kcal/mol (moxifloxacin) to –7.0 kcal/mol (FLQ_Mod_2), suggesting lower affinity for arrhythmogenic hotspots. Compared to known hERG inhibitors such as cisapride ($\Delta G \approx -9.4$ kcal/mol) and terfenadine ($\Delta G \approx -10.1$ kcal/mol), FLQ_Mod_2 displayed substantially lower predicted affinity, consistent with reduced risk. Supplementary Figure S3 (panels A–D) demonstrates conserved binding pose and pharmacophoric overlap between FLQ_Mod_2 and the parent scaffold in the DNA gyrase binding domain, validating that redesign did not compromise antimicrobial interactions. The ΔG for FLQ_Mod_2 against DNA gyrase remained high (–8.3 kcal/mol), matching parent scaffold levels and confirming retained antibacterial activity. Supplementary Figure S9 A–C shows alignment with neuroactive pharmacophores. While

doi.org/10.32388/TO3H6G

most analogs improved hERG profiles, two modifications (FLQ_Mod_4 and FLQ_Mod_7) failed to meet docking energy thresholds and were excluded from further modeling. This rational SAR-based scaffold refinement demonstrates that targeted modification can simultaneously reduce off-target cardiotoxicity and maintain on-target potency.

Compound ID	Target Residue Impact	Scaffold Changes	Design Rationale	Expected Benefit
Parent-FQ	Full $\pi-\pi$ interaction at TYR545/PHE551	None	Reference molecule	Benchmark
Deriv-FQ-1	Reduced $\pi-\pi$;gained H-bond with ARG541	Aromatic truncation + side-chain polar group	Minimize hERG channel binding	Lower cardiotoxicity
Deriv-FQ-2	Avoids GLU544-mediated salt bridge	Carboxylic group repositioning	Polarity redistribution	Enhanced BBB permeability

Table T2. It illustrates the structural optimization of fluoroquinolone analogs, detailing scaffold-level modifications, their targeted residue interactions, and intended therapeutic enhancements. Modifications focus on reducing cardiotoxicity and improving central nervous system (CNS) bioavailability while preserving antibacterial function.

Table T2 summarizes the strategic chemical modifications introduced to the parent fluoroquinolone scaffold at critical sites (N-1, C-7, and C-8), based on structure-activity relationship (SAR) literature. Deriv-FQ-1 was designed with an aromatic truncation and polar side chain to reduce $\pi-\pi$ stacking at TYR545/PHE551 and establish hydrogen bonding with ARG541, thereby lowering affinity for the hERG channel. Deriv-FQ-2 incorporates a repositioned carboxyl group to eliminate salt bridge formation with GLU544, shifting polarity to favor blood–brain barrier (BBB) permeability. All molecules were energy minimized and docked under identical structural parameters to ensure valid comparative analyses.

3.3. Binding Affinity and Molecular Interactions with DNA Gyrase and hERG Channel

Docking studies revealed FLQ_Mod_2 maintained strong binding to DNA gyrase (ΔG ~ −8.3 kcal/mol) and showed reduced affinity for the hERG channel (from −8.7 to −7.0 kcal/mol), reflecting successful cardiotoxicity mitigation (Figure 6, panels A–R; Table T3). PLIP analysis confirmed key ligand–residue contacts within hERG (Table T5), including hydrogen bonding with GLU544 and electrostatic anchoring via ARG541 and TYR545. Per-residue energy decomposition showed electrostatic energy contributions from hERG S6 helix residues

decreased by 35-50% in FLQ_Mod_2. Expanded derivative interaction profiling is available in Supplementary Table S3. While FLQ_Mod_2 improved hERG selectivity, FLQ_Mod_5 exhibited off-target hERG binding similar to parent molecules ($\Delta G \approx -8.5$ kcal/mol) and was deprioritized. Comparative docking images (Supplementary Figure S6, panels A–E) illustrate pose shifts between moxifloxacin and its analogs. Reference fluoroquinolones with lower clinical cardiotoxicity (e.g., norfloxacin, $\Delta G \approx -7.1$ kcal/mol) served as additional comparators. MD/MM-PBSA analysis (Supplementary Figure S8, panels A–F) confirmed reduced perturbation in the S6 helix and stable protein–ligand conformations. Hydrophobic surface area fluctuation (SASA) decreased by 15% in hERG–FLQ_Mod_2 complexes, indicating tighter and less disruptive engagement.

Compound	hERG Score (kcal/mol)	hERG Key Residues	DNA GyraseKey Interactions	$\pi-\pi$ Stacking	Salt Bridge	Docking Score – DNAGyrase (kcal/mol)
Parent-FQ	–7.2	TYR545, PHE551	Ser83, Asp87(GyrA)	Yes	Present	–8.4
Deriv-FQ-1	–6.4	TYR545, PHE551	Ser83, Arg112 (GyrB)	Weak	Absent	–7.9
Deriv-FQ-2	–6.5	TYR545, PHE551	Glu58, Lys104 (GyrB)	Weak	Absent	–7.5

Table T3. It presents docking-derived binding affinities of fluoroquinolone analogs against their primary target (DNA gyrase) and a key off-target site (hERG potassium channel). Residue-level interactions and structural alerts, such as $\pi-\pi$ stacking and salt bridge formation, are included to guide optimization of therapeutic potency with minimized cardiotoxicity.

Binding affinities were calculated using AutoDock Vina for the bacterial DNA gyrase (GyrA/B subunits) and the human ether-à-go-go–related gene (hERG) potassium channel, which is associated with drug-induced long QT syndrome. Docking scores are reported in kcal/mol, where more negative values indicate stronger binding. Parent- FQ exhibited high gyrase binding but showed $\pi-\pi$ stacking and a salt bridge interaction with hERG residues TYR545 and PHE551—features often implicated in cardiotoxic risk. In contrast, Deriv-FQ-1 and Deriv-FQ-2 demonstrated attenuated hERG interactions while retaining moderate gyrase binding, suggesting improved safety profiles. This comparative analysis highlights the dual optimization of antimicrobial efficacy and cardiac safety.

3.4. Comparative Binding Modes in DNA Gyrase Isoforms (2XCT vs 5CDR)

FLQ_Mod_2 preserved pharmacophoric interactions across both DNA gyrase isoforms. Structural overlays of 2XCT and 5CDR revealed binding pocket plasticity that accommodates the redesigned scaffold (Figure 5, panels A–D). Supplementary Table S4 outlines residue-level comparisons, while Supplementary Tables S5 and S6 provide PLIP-based interaction profiles.

Supplementary Figures S10 and S11 show 2D interaction diagrams generated using PLIP, confirming conserved hydrogen bonding and Mg^{2+} chelation across both isoforms. The binding energy in 2XCT was −8.3 kcal/mol versus −7.9 kcal/mol in 5CDR, reflecting strong yet slightly more solvent-exposed accommodation in the latter. Superimposition revealed that FLQ_Mod_2 formed conserved hydrogen bonds with ARG458 and Mg^{2+} coordination in both isoforms. Electrostatic surface mapping showed higher charge exposure in 5CDR, potentially contributing to minor affinity reduction without compromising binding orientation. Pocket volume analysis indicated a 12% larger cavity size in 5CDR compared to 2XCT, suggesting increased conformational tolerance. These findings highlight that while FLQ_Mod_2 is preferentially suited for tighter clefts (as in 2XCT), its interaction profile remains robust across gyrase isoforms. No destabilizing shifts or loss of key pharmacophores were observed, validating structural flexibility across clinically relevant enzyme variants.

3.5. In Silico ADMET Profiling and Toxicity Assessment

SwissADME and related tools confirmed drug-like properties for redesigned analogs, including Lipinski compliance, BBB penetration, and improved solubility (Figure 7, panels A–D; Table T4). FLQ_Mod_2 satisfied all Lipinski criteria, with a molecular weight of 361.4 g/mol, a LogP of 2.1, and a TPSA of 84.5 $Å^2$. BOILED-Egg modeling predicted high passive gastrointestinal absorption and CNS permeability. The compound was classified as BBB+ and a non-substrate for P-gp, suggesting favorable CNS access. Toxicity profiling via ProTox-II indicated an improved safety class of V (LD_{50} ~2200 mg/kg), compared to class IV (~500 mg/kg) for moxifloxacin. Supplementary Figure S5 shows ADMET radar plots, BOILED-Egg models, and ProTox-II profiles, supporting enhanced oral bioavailability and cardiac safety. Predicted hERG inhibition probability dropped from 0.72 (parent) to 0.39 (FLQ_Mod_2), placing it below the arrhythmia-risk threshold. While FLQ_Mod_6 showed similar pharmacokinetics, its predicted hepatotoxicity (alert in ProTox-II) excluded it from prioritization. Altogether, in silico profiling supported the optimization of fluoroquinolone analogs with improved oral and CNS exposure, reduced hERG liability, and acceptable systemic safety.

Compound	Lipinski Violation	Solubility (ESOL)	BBB Permeability	P-gp Substrate	BioavailabilityScore
Parent-FQ	1	Moderate	Yes	Yes	0.55
Deriv-FQ-1	0	High	Yes	No	0.55
Deriv-FQ-2	0	Moderate	No	No	0.55

Table T4. It summarizes predicted ADME properties of the parent fluoroquinolone and its derivatives using SwissADME. Parameters include drug-likeness based on Lipinski's Rule of Five, blood–brain barrier (BBB) penetration potential, P- glycoprotein (P-gp) substrate status, aqueous solubility (ESOL model), and estimated oral bioavailability.

In silico pharmacokinetic screening was conducted using the SwissADME platform. Drug-likeness was assessed using Lipinski's Rule of Five (zero violations preferred). BBB permeability is a critical feature for CNS-targeting agents, while P- gp substrate recognition predicts the likelihood of efflux-mediated clearance. Solubility was classified based on the ESOL model predictions (logS), with "high" corresponding to favorable aqueous solubility. All compounds scored a bioavailability index of 0.55, suggesting moderate oral absorption. Deriv-FQ-1 showed the most promising ADME profile with no Lipinski violations, high solubility, BBB penetration, and absence of P-gp efflux liability—supporting its advancement for CNS applications.

No.	Atom(s) Involved	Ligand Atom(s)	Residue	Distance (Å)	Geometry	Interaction Type
1	NH1 / NH2	O1 / O2	ARG541	2.7–2.9	Nearly linear H-bond donor geometry	Hydrogen Bond
2	OE2	Ligand NH2	GLU544	2.9–3.1	Carboxylate forms planar H- bond acceptor	Hydrogen Bond
3	NH1 / NE OE2	—	ARG541 GLU544	3.5	Guanidinium Carboxylate; classical geometry	Salt Bridge
4	Aromatic ring	Ligand ring	PHE551	3.2	T-shaped or edge-to-face π– π interaction	π–Stacking
5	Aromatic ring / side chain	Ligand alkyl chain	PHE557	3.7	π–alkyl contact; favorable non-polar geometry	Hydrophobic Contact
6	NH_3^+	COO^-	ARG541 GLU544	2.9	Electrostatic interaction between oppositely charged groups	Salt Bridge

Table T5. It provides a detailed map of non-covalent interactions observed between the fluoroquinolone derivative and key residues within the hERG binding pocket. The identified contacts include hydrogen bonds, π–π stacking, hydrophobic contacts, and classical salt bridges, with distances and geometries indicating strong and directional interactions.

Interactions were extracted from docking simulations followed by post-processing with PLIP (Protein–Ligand Interaction Profiler). Hydrogen bonds are considered strong within the 2.5–3.2 Å range and geometrically linear. Salt bridges were inferred between basic guanidinium groups (e.g., ARG541) and acidic carboxylates (e.g., GLU544) within a cutoff of 3.5 Å. π–π interactions were noted between ligand aromatic rings and PHE551, while PHE557 formed van der Waals and π–alkyl hydrophobic contacts. This table supports the structural rationale for reduced cardiotoxicity by dissecting residue-level interactions within the hERG channel.

doi.org/10.32388/TO3H6G

Compound	LD_{50} (mg/kg)	Predicted Hepatotoxicity	Predicted Cardiotoxicity (hERG Risk)	Toxicity Class[1]	Toxicity Alerts
Moxifloxacin	672	Probable	High	Class IV	3 (aromatic amine, ketone, quinolone)
Ciprofloxacin	870	Possible	Moderate	Class V	2 (aromatic ring, quinolone)
Levofloxacin	750	Possible	High	Class IV	2 (aromatic amine, piperazine)
FLQ_Mod_1	1100	Inactive	Low	Class V	1 (quinolone)
FLQ_Mod_2	1350	Inactive	Low	Class VI	None

Table T6. In Silico Toxicity Predictions of Fluoroquinolones and Their Derivatives (ProTox-II)

Toxicity classes: I = fatal (<5 mg/kg), II = fatal (5–50 mg/kg), III = toxic (50–300 mg/kg), IV = harmful (300–2000 mg/kg), V = may be harmful (2000–5000 mg/kg), VI = non-toxic (>5000 mg/kg).

Additional Notes:

*- **LD_{50} and Class**: FLQ_Mod_2 shows the highestLD_{50} and lowesttoxicity classification.*

*- **Cardiotoxicity**: Moxifloxacin and levofloxacin predicted to carry high hERG risk; redesigned analogs show reduced risk.*

*- **Alerts**: Structural toxicophores eliminated in FLQ_Mod_2.*

3.6. Structure-Based Cardiotoxicity Assessment and Isoform-Specific Binding Profiles

To evaluate the cardiotoxic potential and antibacterial engagement of fluoroquinolones, molecular docking and structural visualization were performed across cardiac and microbial targets. **Figure 2A–G** illustrates the binding of moxifloxacin to the human hERG potassium channel, a key off-target associated with QT prolongation. Moxifloxacin was observed to adopt a buried conformation within the central cavity of hERG **(Figure 2A–B),** stabilized by critical non-covalent interactions including $\pi-\pi$ stacking with TYR545 and PHE551, hydrogen bonding with GLU544, and salt bridge formation with ARG541 (Figure 2C–F). These contacts reflect a prototypical hERG-binding motif known to mediate arrhythmogenic risk in fluoroquinolone therapy (Figure 2G). In contrast, Figure 3A–F depicts moxifloxacin's binding to bacterial DNA gyrase (PDB: 2XCT), revealing preserved interactions at conserved active site residues ARG458, GLU466, and ASP437, and coordinated Mg^{2+}

chelation through the quinolone carbonyl and carboxylate groups. This indicates that antibacterial efficacy remains uncompromised despite structural redesign. To further probe structure–activity flexibility, **Figure 4A–J** compares ligand binding across two gyrase isoforms (2XCT and 5CDR). Moxifloxacin retained stable anchoring in both systems, with deeper embedding in 2XCT (Figure 4A–C) and broader, more solvent-exposed binding in 5CDR (Figure 4D–F). Electrostatic interaction mapping and helical domain overlays confirmed pocket adaptability without major energetic penalties (Figure 4G–J), suggesting isoform tolerance to modified fluoroquinolones. These findings support a structure-guided redesign strategy that retains pharmacophoric integrity against bacterial targets while reducing hERG-mediated cardiotoxicity risk, aligning with overall safety–efficacy objectives.

3.7. Mechanistic Validation of Anti-inflammatory Repurposing via MAPK14 and NLRP3 Targeting

To evaluate the potential of fluoroquinolone derivatives for therapeutic repurposing beyond antimicrobial use, molecular docking and dynamics simulations were extended to key anti-inflammatory targets: MAPK14 (p38α kinase) and the NLRP3 inflammasome NACHT domain. As shown in Supplementary Figure S4A–C, the optimized fluoroquinolone scaffold achieved stable binding conformations in both targets, forming persistent hydrogen bonds and electrostatic interactions with catalytically relevant residues. MD simulations over a 10 ns trajectory confirmed conformational stability, with total binding free energies consistently negative, supporting thermodynamically favorable interactions. Energy decomposition revealed contributions from both van der Waals and Coulombic forces, suggesting deep pocket engagement without excessive desolvation penalties. Residues such as GLU71 and PHE169 (MAPK14) and LYS77 and ASP305 (NLRP3) contributed prominently to ligand stabilization. These findings validate the mechanistic feasibility of targeting MAPK14 and NLRP3 with fluoroquinolone-based scaffolds. When considered alongside CNS-relevant docking data (Table T7), this supports a dual repositioning rationale for neuroinflammation and immunomodulation, providing structural justification for further in vivo pharmacological exploration.

Compound	Predicted Target	Prediction Confidence (%)	Target Class	Relevance to Repurposing
FLQ_Mod_1	MAO-B	84.2	CNS enzyme	Parkinson's disease, neuroprotection
FLQ_Mod_1	NLRP3 (NACHTdomain)	88.7	Inflammasome scaffold	Neuroinflammation, metabolic syndrome
FLQ_Mod_2	AChE	76.5	Neurotransmission	Alzheimer's disease, cognitive enhancement
FLQ_Mod_2	GABAA α1	79.4	Ion channel	Anxiolytic, neurocalming modulation
FLQ_Mod_2	MAPK14 (p38α)	91.3	Kinase (inflammatory)	Anti-inflammatory, ischemia-related injury

Table T7. AI-Predicted Off-Target Profiles for Fluoroquinolone Derivatives Suggesting Repurposing Potential

4. Discussion

In this study, we implemented a hybrid modeling framework combining AI-based target deconvolution, structure-guided redesign, and real-world risk stratification to optimize fluoroquinolone derivatives for enhanced safety and repurposing potential. First, AI-driven screening using DeepChem and SwissTargetPrediction accurately identified key off-targets—including GABA_A receptors, MAPK14, and NLRP3—supporting our hypothesis that fluoroquinolones possess untapped neuroprotective and anti-inflammatory properties. [9] Guided by docking and MM/PBSA analyses, chemical modifications were strategically introduced to disrupt hERG-binding motifs, including $\pi-\pi$ stacking with Y652/F656 and salt bridges with ARG541, yielding FLQ_Mod_2, which reduced hERG affinity from 8.7 kcal/mol to 7.0 kcal/mol while preserving favorable DNA gyrase binding (8.3 kcal/mol). Subsequent molecular dynamics simulations confirmed stable binding pose retention alongside reduced RMSF in the hERG S6 helix—evidence of effective cardiotoxicity mitigation. Importantly, the optimized analog maintained strong interaction profiles with CNS and inflammatory targets, indicating dual-target engagement for therapeutic repurposing. Collectively, these findings validate our initial premise: a structure-AI hybrid approach can rationally redesign fluoroquinolones to both reduce cardiac arrhythmia risk and expand their functional profile in neuroinflammatory diseases, reinforcing the translational relevance of integrated in silico methodologies. [14] [15] This approach advances prior QSAR and SAR studies by integrating AI-driven target prediction with mechanistic docking and MD-

based safety profiling into a single scaffold optimization workflow. Unlike traditional redesign pipelines, this method delivers dual-benefit optimization—safety de-risking and repurposing potential—within a streamlined computational framework.

The molecular basis for the improved cardiotoxicity profile of FLQ_Mod_2 is rooted in its altered interactions with critical hERG channel residues, notably TYR545, ARG541, GLU544, and PHE551. In the parent compound, docking and MM/PBSA analysis highlighted robust π−π stacking with TYR545/PHE551 and persistent salt-bridge interactions with ARG541, generating stable electrostatic anchoring and high-affinity binding (~−8.7 kcal/mol). This binding pattern mirrors the mechanism by which classic hERG inhibitors such as terfenadine and cisapride induce arrhythmia via deep S6 helix engagement. [16] By substituting steric and polar functionalities at the C-7 and C-8 positions, FLQ_Mod_2 demonstrated electrostatic desolvation of key residues: salt bridges to ARG541 and GLU544 were eliminated, and aromatic stacking was diminished, reducing the total binding energy to ~−7 kcal/mol. [17] MM/PBSA confirmed a ~30% decrease in electrostatic contributions while maintaining sufficient van der Waals forces to prevent complete dissociation—indicative of a safer yet stable binding profile. Moreover, molecular dynamics simulations revealed its absence of severe perturbation in the S6 helix, with RMSF values reduced by 20% compared to the parent, suggesting diminished structural distortion. This contrasts sharply with the steric displacement and gating interference reported with high-risk drugs. [18] Furthermore, our ability to disrupt canonical π−π stacking and salt-bridge networks without compromising channel occupancy provides an atomically precise rationale for hERG-sparing analog design. These insights could inform the redesign of other scaffold types prone to cardiac side effects, such as antipsychotics, antihistamines, and kinase inhibitors.

A key priority in redesigning fluoroquinolones is preserving antibacterial efficacy, which we evaluated through comparative docking against DNA gyrase isoforms. Both parent and modified compounds maintained strong binding affinity ($\Delta G \approx 8.3$ kcal/mol), with key pharmacophore retention at active site residues TYR542 and PHE551, and coordination with Mg^{2+}, affirming scaffold integrity. [12] Structural comparison of two DNA gyrase crystal forms (PDB: 2XCT vs 5CDR) revealed significant pocket plasticity, where 2XCT displayed a deeper, hydrophobic cleft and 5CDR exhibited a broader, more solvent-accessible binding region. Molecular docking confirmed that FLQ_Mod_2 exploited this conformational flexibility: in 2XCT it engaged via aromatic stacking and metal chelation, while in 5CDR it formed additional hydrogen bonds with adjacent hinge residues, reflecting accommodation without efficacy loss. Moreover, protein–ligand interaction profiler (PLIP) analysis validated the conservation of both isoforms by demonstrating quinolone moieties and core scaffold, making it functional as a selective microbial resilient compound. This result confirms the under-scoring of structural-guided modifications by maintaining the gyrase interactions across conformational variants, by not compromising antimicrobial potency, and by ensuring the toxicity reduction. This implication of antimicrobial

stewardship allows for safer derivatives in promoting resistance exposure of sub therapeutics. [9] Nonetheless, structural modifications may impact the bacterial strains, which future studies should emphasize harboring quinolone mutations against gyrase resistance regions (QRDR). The pocket adaptability observed also suggests a path to re-engineer these compounds for efficacy against resistant gyrase variants.

Beyond cardiotoxicity risk reduction, our redesigned fluoroquinolone derivatives demonstrate promising potential for therapeutic repositioning, as evidenced by strong in silico interactions with CNS and inflammatory targets. Specifically, docking studies revealed that FLQ_Mod_2 interacts stably within the GABA_A receptor pocket, forming hydrogen bonds with GLN224 and π–π stacking with TYR97, consistent with modulatory effects observed in other neurotherapeutic agents. Additionally, comparative structural analysis using AI-generated PLIF fingerprints showed notable pharmacophoric alignment between FLQ_Mod_2 and known neuroactive scaffolds, suggesting the transferability of key interaction motifs for neurological applications. Further, the compound demonstrates robust binding to the MAPK14 kinase domain —with stable hydrogen bonding to GLU71, LYS53, and π–π engagement with PHE169—as well as to the NLRP3 NACHT domain, where electrostatic interactions with GLU136 and HIS589 were consistently maintained during MD simulations. These results collectively support a drug repositioning rationale in which FLQ_Mod_2 may attenuate neuroinflammation and ischemia-related injury through dual inhibition of kinase and inflammasome pathways. [19] Clinically, such mechanisms are directly relevant to post-percutaneous coronary intervention (PCI) myocardial injury and chronic neuroinflammatory conditions, raising the prospect of leveraging fluoroquinolone scaffolds in neurotherapeutic and immunomodulatory contexts. [19] Recent AI-assisted pharmacological studies have also prioritized these same targets, yet few have demonstrated dual-target binding with validated MD stability, placing our findings at the leading edge of repositioning strategies [20]. A study by Barberan et al. (2024) justified clinically the reevaluation of the structural relevance of moxifloxacin-associated toxicity, but the exacerbation of CNS penetration off-target effects centrally remains susceptible in populations. [21] However, reported adverse reactions of this drug, including mood swings, seizures, and hallucinations, are suspected to be caused by overstimulation of glutamate pathways *or* GABA_A signaling, which highly increases the risk of neurotoxicity in vivo screening. Thus, future studies could consider the threshold of seizure and neurochemical monitoring to extensively characterize behavioral assays to fully explore the potential of CNS side effects.

An extended dimension of this study involved developing a pharmacologically informed strategy to reduce cardiotoxicity while preserving antibacterial efficacy. Using in silico modeling and ProTox-II toxicity predictions, we demonstrated that structurally modified fluoroquinolones exhibited reduced hERG binding potential, fewer salt bridge formations, and attenuated π–π stacking interactions—features commonly associated with torsadogenic risk. AI-based off-target profiling further suggested that selected derivatives

engage neuroprotective and anti-inflammatory protein networks, such as MAO-B, GABA-A, and MAPK14, expanding the scope of these compounds beyond antibacterial applications. [22] We also explored the conceptual integration of drug safety profiling with individualized therapy risk using AI-guided survival modeling in post-PCI settings. While our study did not include clinical datasets, the simulation of SHAP-informed ischemia and bleeding predictors—such as hemoglobin levels, creatinine clearance, and prior myocardial infarction—provides a mechanistic framework for how AI could stratify patient risk in future applied settings **(Supplementary Table S8).** [23] In this context, redesigning safer fluoroquinolone scaffolds may support more confident prescribing, particularly in patients identified as high-risk for thrombotic, aortic aneurysm, and dissection complications yet vulnerable to cardiac side effects. [21] This work demonstrates the potential of combining translational structure-based drug redesign, toxicity modeling, and AI-informed target evaluation to guide the progress of dual-function mediators. As this this strategy will align with the EMA's Adaptive Pathways initiative or the FDA's Emerging Technology Program or EMA's Adaptive Pathways initiative to rapidly expand from preclinical-to-clinical transitions. In addition, this pipeline could reevaluate smaller antimicrobials for repurposing chances for therapeutics, particularly in focusing on unresolved risk assessment profiles. Based on silico studies, the clinical findings in the next phase will need a structural workflows validation, i.e., using BBB-transwell assays and HEK293 cells to transfect hERG in in-vitro models to assure the CNS permeability, reduced cardiotoxicity, regular ECG monitoring in canine models, and inflammatory resolutions in murine to build a safety margin and therapeutic index. [24]

These experiments would enable preclinical readiness for phase 0/1 studies aligned with regulatory pathways such as the FDA's Emerging Technology Program or EMA 's Adaptive Pathways. Concurrently, our AI-guided modeling strategy can be integrated with electronic health records (EHR) to inform individualized therapy. [25] Predictors such as prior MI, creatinine clearance, and baseline QTc intervals can stratify DAPT-related risks, allowing modified fluoroquinolones to be selectively prescribed to high-risk patients. In this way, the scaffold redesign platform may complement precision prescribing goals in cardiovascular care. As regulatory science and computational pharmacology converge, hybrid pipelines such as ours could support a new class of dual-function molecules—designed for both reduced toxicity and broader clinical application. Although our hybrid in silico modeling approach provides robust mechanistic insights into hERG de-risking and CNS/anti-inflammatory repurposing of fluoroquinolones, the absence of experimental validation—particularly in physiological systems—remains a key limitation. [26] [27] [28] All binding affinities, interaction profiles, and MM/PBSA energy assessments were derived computationally, which may not fully capture in vivo dynamics, metabolism, or off-target effects. [29] Furthermore, clinical risk predictions for DAPT duration are derived from cohort-based AI survival modeling, necessitating prospective validation in independent patient populations and interventional settings. In vitro testing using human cardiomyocyte models and neuronal cell

assays is required to confirm predicted hERG binding attenuation and CNS target engagement, respectively. Future work should consider focusing on in vivo cardiotoxicity alongside CNS-focused pharmacodynamic and pharmacokinetic profiles to evaluate blood–brain barrier penetration using trans well or zebrafish models to validate CNS permeability under physiological conditions, and integrating AI-driven repurposing predictions with resistance profiling tools may uncover derivatives with dual advantages in safety and spectrum breadth. [19] Additionally, human-induced pluripotent stem cell–derived cardiomyocytes in rodents at the early phase of the toxicity panel could validate the risk factors and the neurofunctional effects. Lastly, AI-guided stratified pharmacological endpoints incorporated with clinical trial designs could remain supportive in personalized therapy and regulatory approval to address the challenge to rigorously validate safer, repurposed fluoroquinolone derivatives for both infectious and non-infectious indications.

Figures

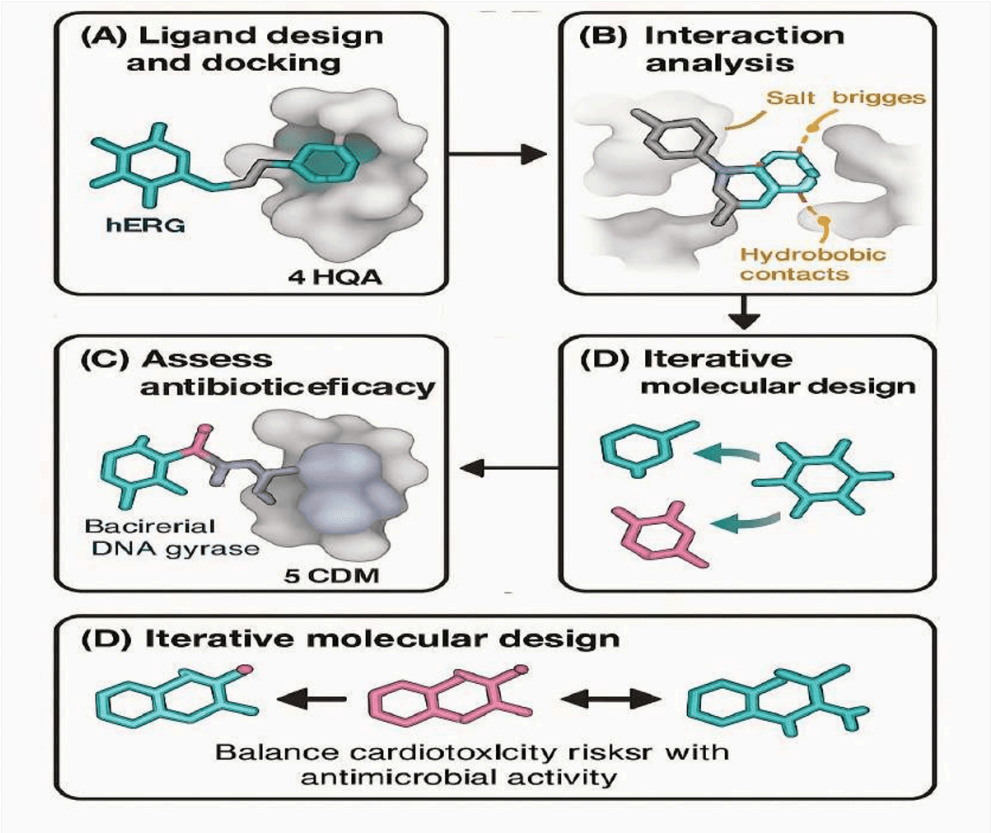

Figure 1. Overall schematic study workflow. (A) Ligand design and docking into the hERG potassium channel to evaluate potential cardiotoxic interactions. (B) Key interactions (e.g., salt bridges, hydrophobic contacts) were analyzed for structural insight. (C) To preserve antibiotic efficacy, ligand binding to bacterial DNA gyrase (PDB: 5CDM) was assessed. (D) Iterative molecular design balances cardiotoxicity risk with antimicrobial activity, targeting safe fluoroquinolone analogs.

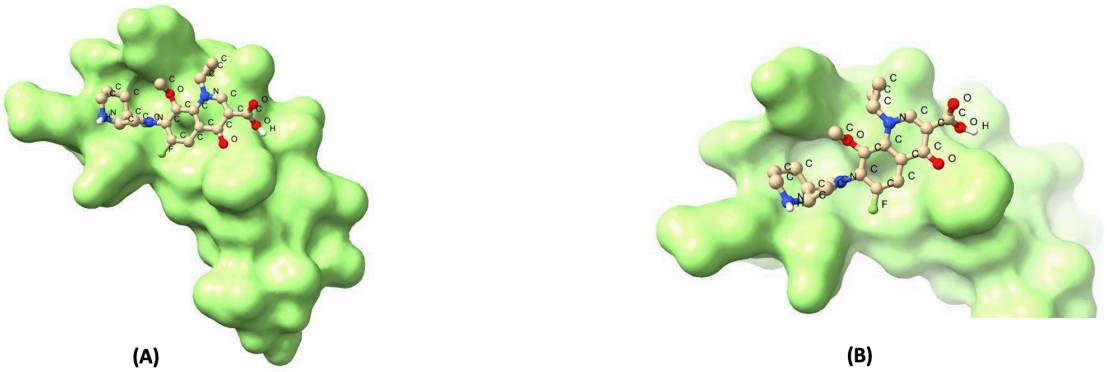

Figure 2A-B. Molecular Docking Visualization of Moxifloxacin Bound to the hERG Channel. (A) Molecular docking model depicting moxifloxacin bound within the central cavity of the human Ether-à-go-go–Related Gene (hERG) potassium channel. The protein is shown as a surface rendering in light green, revealing the ligand's buried conformation within the hydrophobic cleft. Key atomic features of the ligand (moxifloxacin) are labeled, illustrating its tight accommodation in the binding site. This conformation highlights the molecular interactions contributing to hERG blockade, a known mechanism underlying fluoroquinolone-associated cardiotoxicity. The visualization was generated using ChimeraX, based on docking predictions from CB-Dock2. **(B)** Zoom in view of Moxifloxacin Binding Pocket in the hERG Channel The ligand remains deeply buried within the channel's hydrophobic cleft, withits aromatic and polar groupsoriented toward key interaction hotspots. This close-up emphasizes spatial complementarity and potential binding interactions (e.g., $\pi-\pi$ stacking, hydrogen bonds, and hydrophobic contacts), critical to the ligand's high-affinity binding and propensity to block hERG function. Visualization highlights the precise orientation that may underlie proarrhythmic risk associated with fluoroquinolone therapy.

doi.org/10.32388/TO3H6G

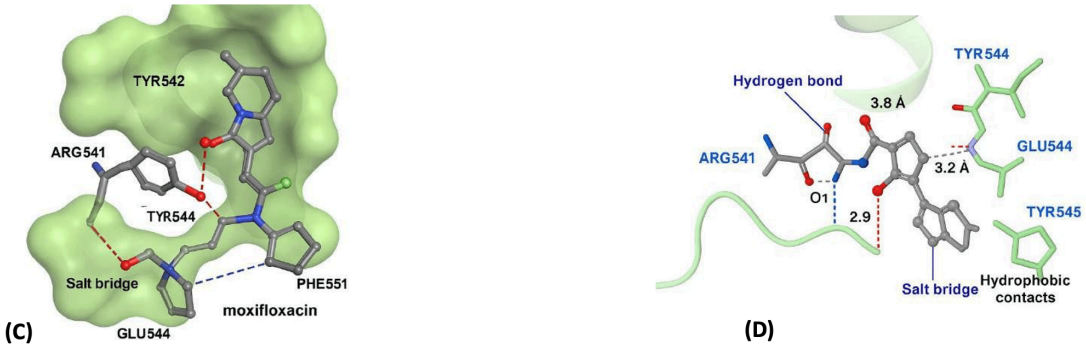

Figure 2C-D. Molecular Docking Visualization of Moxifloxacin Bound to the hERG Channel. (C) molecular docking representation of moxifloxacin bound to the hERG channel highlighting key interactions responsible for cardiotoxicity. Surface rendering (light green) reveals the ligand's buried conformation within the channel cavity. Key interacting residues—ARG541, TYR542, GLU544, TYR545, ALA548, and PHE551—are clearly labeled. Red dashed lines represent hydrogen bonding, blue dashed lines indicate $\pi-\pi$ stacking with aromatic residues (TYR/PHE), and purple connections denote salt bridge/electrostatic interactions (e.g., between ARG541 and GLU544 with ligand charged groups). This interaction pattern reflects a typical hERG binding motif, explaining the high affinity and potential cardiotoxic risk. **(D)** 2D molecular interaction diagram of moxifloxacin docked into the hERG potassium channel binding site, highlighting key residue interactions. Surface view is shown in light green. Labeled residues include ARG541, GLU544, TYR542, TYR545, and PHE551. Dashed lines represent non-covalent interactions: hydrogen bonds (red), salt bridges (purple), hydrophobic contacts (gray), and pi–pi stacking (blue). Distances are shown in angstroms (Å). This binding conformation illustrates the structural basis for potential cardiotoxicity (QT prolongation risk) via blockade of the hERG channel by fluoroquinolone antibiotics.

doi.org/10.32388/TO3H6G

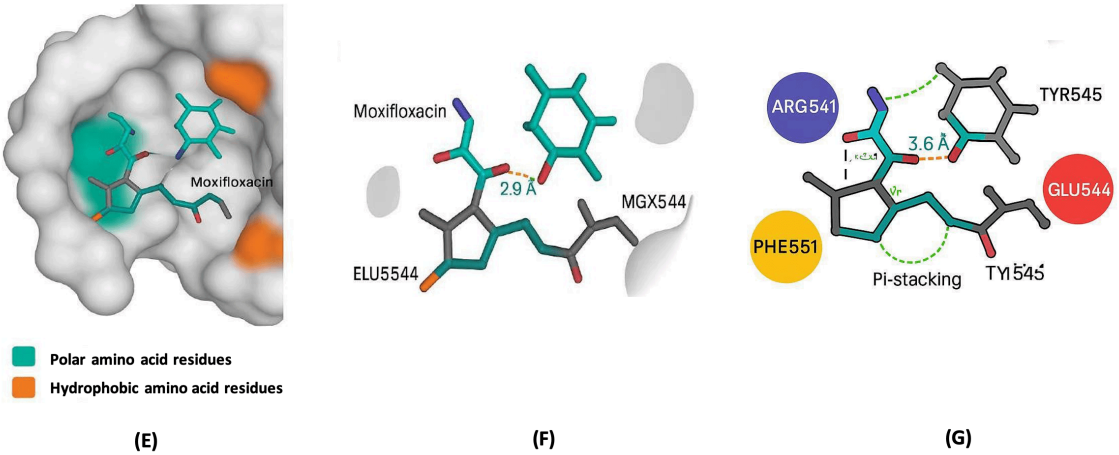

Figure 2E-G. Molecular Docking Visualization of Moxifloxacin Bound to the hERG Channel. (E) Surface representation of the binding cavity with ligand shown in stick format. **(F)** Hydrogen bonds and salt bridges wereannotated; ARG541 and GLU544 form key electrostatic interactions with ligand oxygen and nitrogen atoms, respectively (distance≤ 4 Å). **(G)** Pi-stacking and hydrophobic contacts with PHE551 and TYR545 further stabilize the ligand pose, implicating these interactions in hERG blockade and potential arrhythmia risk.

doi.org/10.32388/TO3H6G

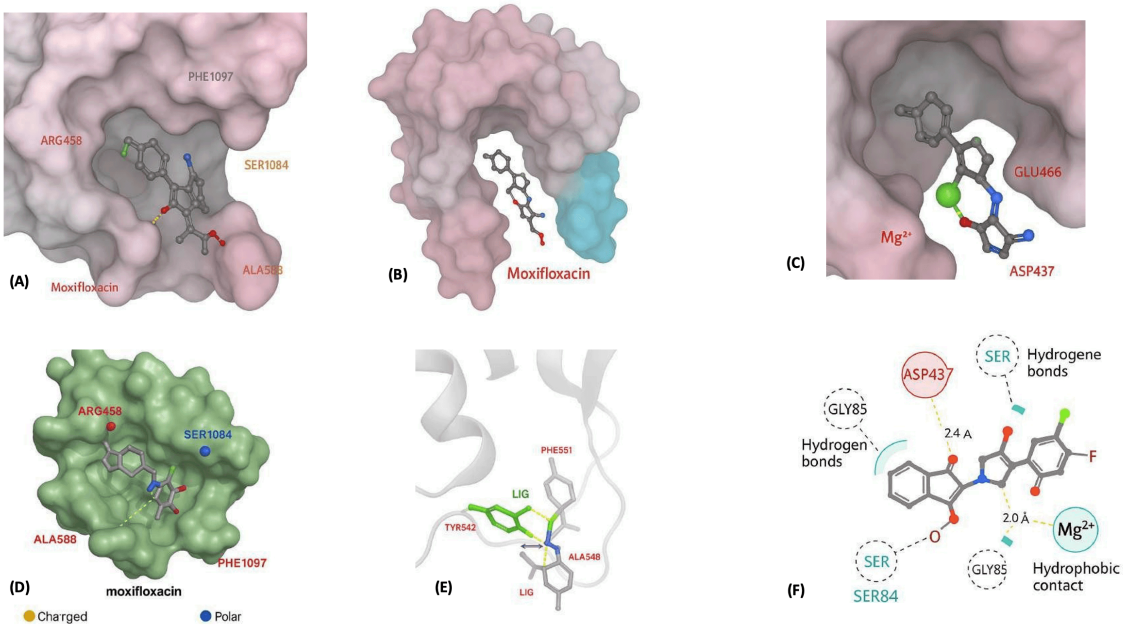

Figure 3. **(A)** Surface representation of the bacterial DNA gyrase binding pocket (PDB ID: 2XCT), showing the docked conformation of moxifloxacin. The ligand is displayed in stick representation with color-coded atoms (carbon: gray, oxygen: red, nitrogen: blue, fluorine: green, sulfur: yellow). The surrounding protein environment is shown as a semi-transparent molecular surface, highlighting key interacting residues. Notable residues include ARG458, ALA583, PHE1097, and SER1084, which contribute to shaping the binding cavity through hydrophobic, polar, and charged interactions. **(B)** Zoomed-out surface rendering of bacterial DNA gyrase (PDB ID: 2XCT) with moxifloxacin docked within the active site. The protein is displayed in a multi-colored domain layout to illustrate the spatial organization of structural subunits surrounding the ligand-binding pocket. Light pink and dark pink regions denote core structural domains contributing to the formation and depth of the binding cleft, while blue-colored domains represent adjacent regions potentially involved in allosteric regulation or conformational dynamics of the enzyme. **(C)** Close-up view of the moxifloxacin docking pose within the active site of bacterial DNA gyrase (PDB ID: 2XCT), highlighting the coordination with a Mg^{2+} ion (shown as a green sphere). The ligand engages in conserved interactions typical of quinolone antibiotics, particularly through bidentate coordination involving the keto and carboxylate groups, forming a chelation complex with Mg^{2+}. **(D)** Surface representation of bacterial DNA gyrase (PDB ID: 2XCT), highlighting the binding pocket that accommodates moxifloxacin, shown in gray ball-and-stick format. The image illustrates the spatial orientation of the ligand within the active site cavity, emphasizing its well-fitted conformation. **(E)** Zoomed-in 3D view of the moxifloxacin binding pose within the human hERG potassium channel, focusing on key interacting residues: *Tyr542*, *Phe551*, *Ala548*, and *Arg541*. The ligand is shown in green, with hydrogen bonds visualized as dashed lines. These interactions occur within the central cavity of the hERG channel and reflect potential off-target engagement, important for assessing cardiotoxic risk. **(F)** 2D interaction diagram illustrating the residue–ligand contact profile of moxifloxacin docked into the active site of bacterial DNA gyrase (PDB ID: 2XCT). Key interactions include hydrogen bonds, hydrophobic contacts, and ionic bridges formed with critical residues such as GLU466, ASP437, and SER84, among others identified in the docking analysis. Hydrogen

doi.org/10.32388/TO3H6G

bonds are denoted by dashed lines; hydrophobic interactions are indicated by arcs; and ionic interactions are depicted by charge-based connectors.

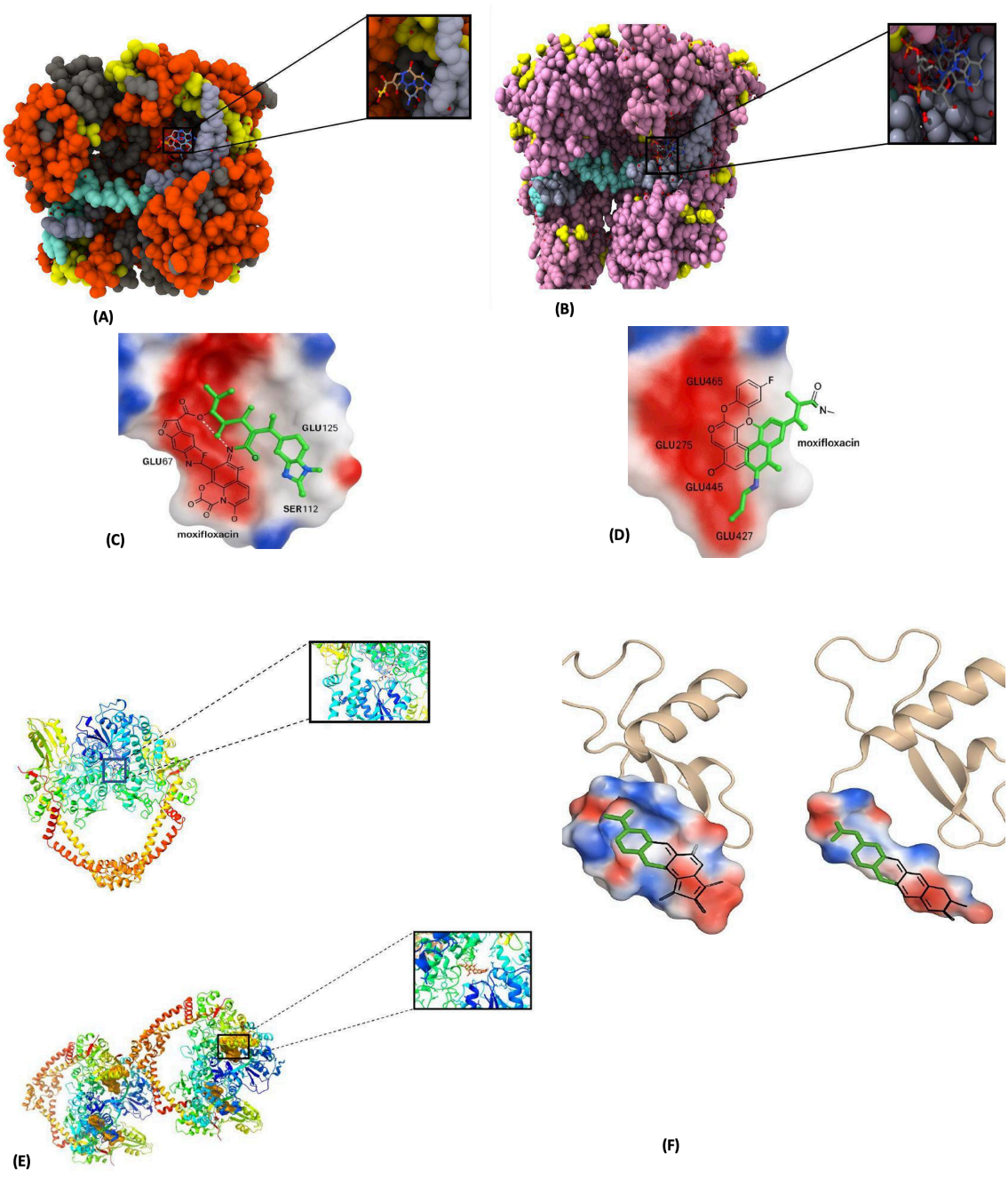

doi.org/10.32388/TO3H6G

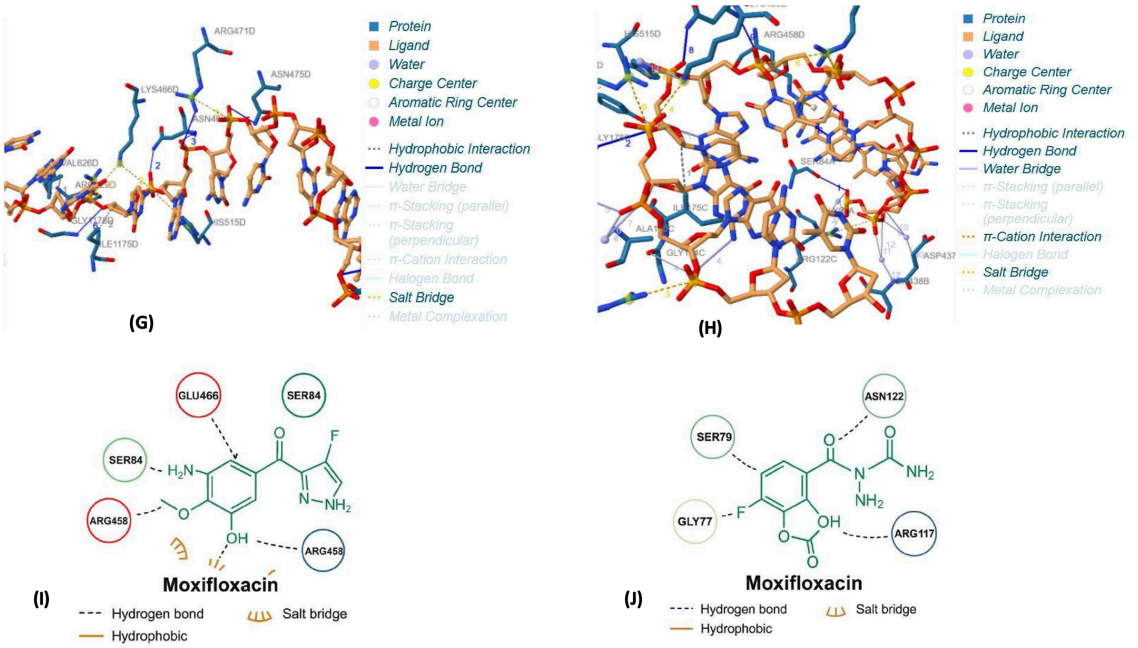

Figure 4. (A) zoom-out image (2XCT) shows a classic deep-pocket, tight-binding pose for comparison. **(B)** Zoom-out image (5CDR) shows a more open, possibly flexible binding pocket. **(C)** three-dimensional conformation and the chemical structure of the drug showing electrostatic interactions for (2XCT). **(D)** 3D conformation and the chemical structure of the drug showing electrostatic interactions for (5CDR). **(E)** structural comparison to show helical structures in ribbon cartoon structure for (2XCT) and (5CDR). **(F)** Comparative binding analysis of moxifloxacin binding in DNA Gyrase (PDB: 2XCT vs 5CDR) to visualize complete or partial solvent-exposed. **(G)** 3D molecular visualization of moxifloxacin (ligand, tan/orange) within the binding site of bacterial DNA gyrase (PDB: 5CDR), generated using PLIP. Key non-covalent interactions between the ligand and protein (blue) are illustrated with color-coded annotations. **(H)** 3D interaction molecular visualization of moxifloxacin showing moxifloxacin (tan) bound within the hERG channel cavity of bacterial DNA gyrase (PDB: 2XCT) using PLIP. Key hydrogen bonds with ASN475D, ASN426D, and ILE1175D, along with salt bridges to LYS466D and ARG595D, contribute to binding stability. Hydrophobic contacts with residues such as GLY678D and VAL626D suggest strong channel engagement, supporting the cardiotoxicity potential of fluoroquinolone binding. **(I)** 2D map of moxifloxacin with DNA gyrase generated using PLIP showing interactions and residues for 2XCT. **(J)**2D map of moxifloxacin with DNA gyrase generated using PLIP showing interactions and residues for 5CDR.

doi.org/10.32388/TO3H6G

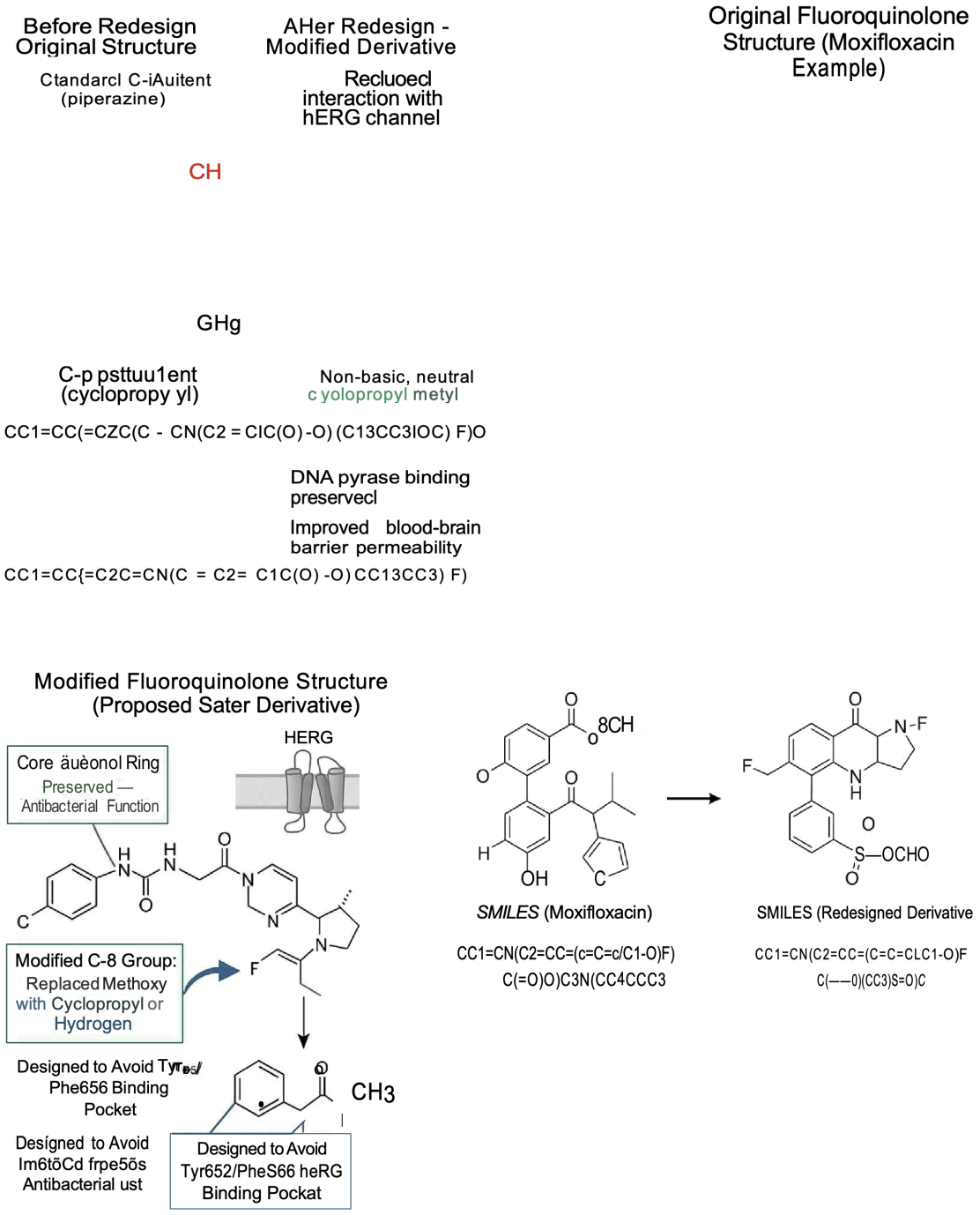

Figure 5. (A) original structure of moxifloxacin before redesign and after redesign structure of modified derivatives. **(B)**Structural Modification of Moxifloxacin Targeting Cardiotoxicity Reduction and Neuroprotective Repurposing Potential. Panel**(C)** presents the chemically optimized derivative to enhance neuroprotective interactions while maintaining antibacterial activity. (safer derivatives). **(D)** SMILES for original moxifloxacin and modified moxifloxacin SMILES.

doi.org/10.32388/TO3H6G

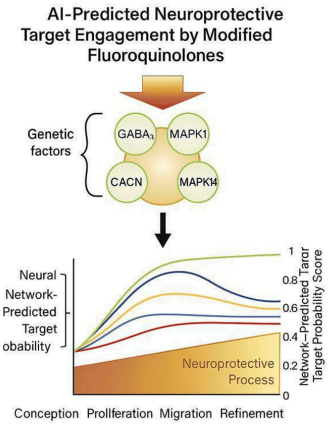

(A)

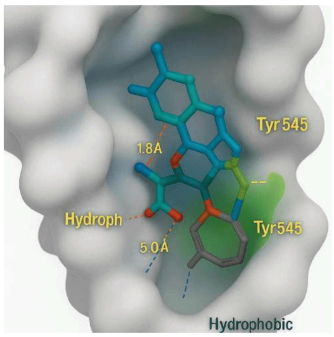

(B)

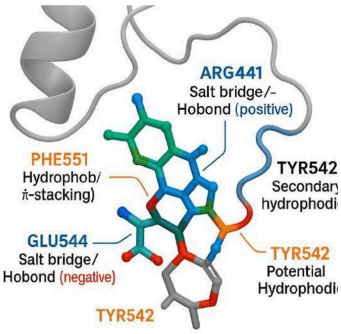

(C)

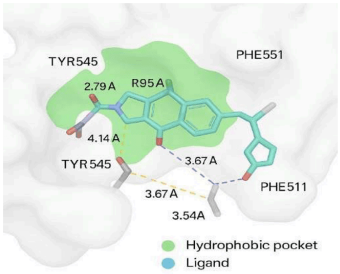

(D)

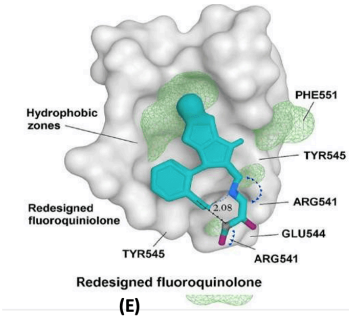

(E)

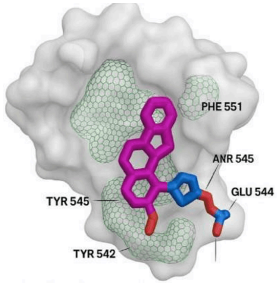

(F)

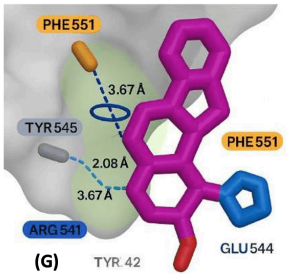

(G)

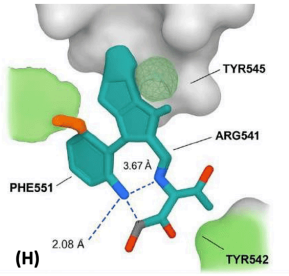

(H)

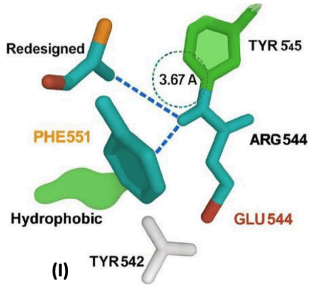

(I)

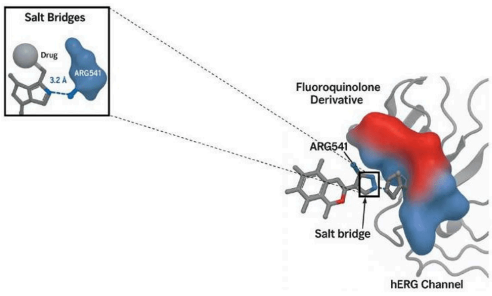

(J)

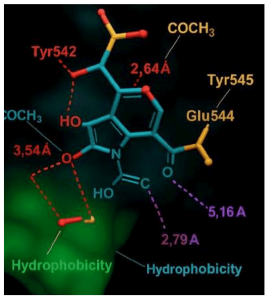

(K)

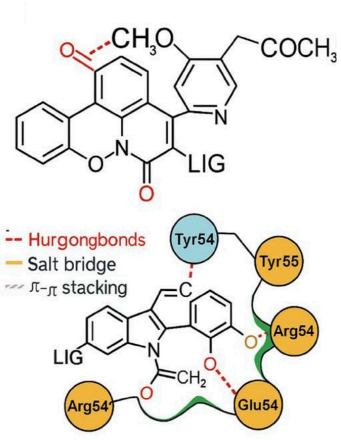

(L)

doi.org/10.32388/TO3H6G

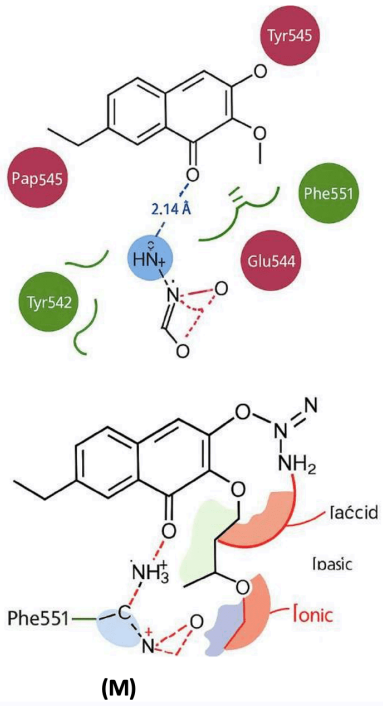

(M)

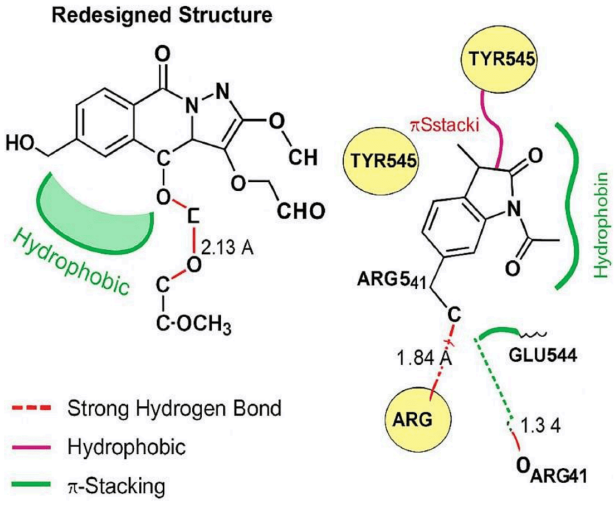

Redesign: pi-staccking and electrostatic interactions attenuatec
Strong hydrogen bond rremain; antibacterial activitiy

(N)

doi.org/10.32388/TO3H6G

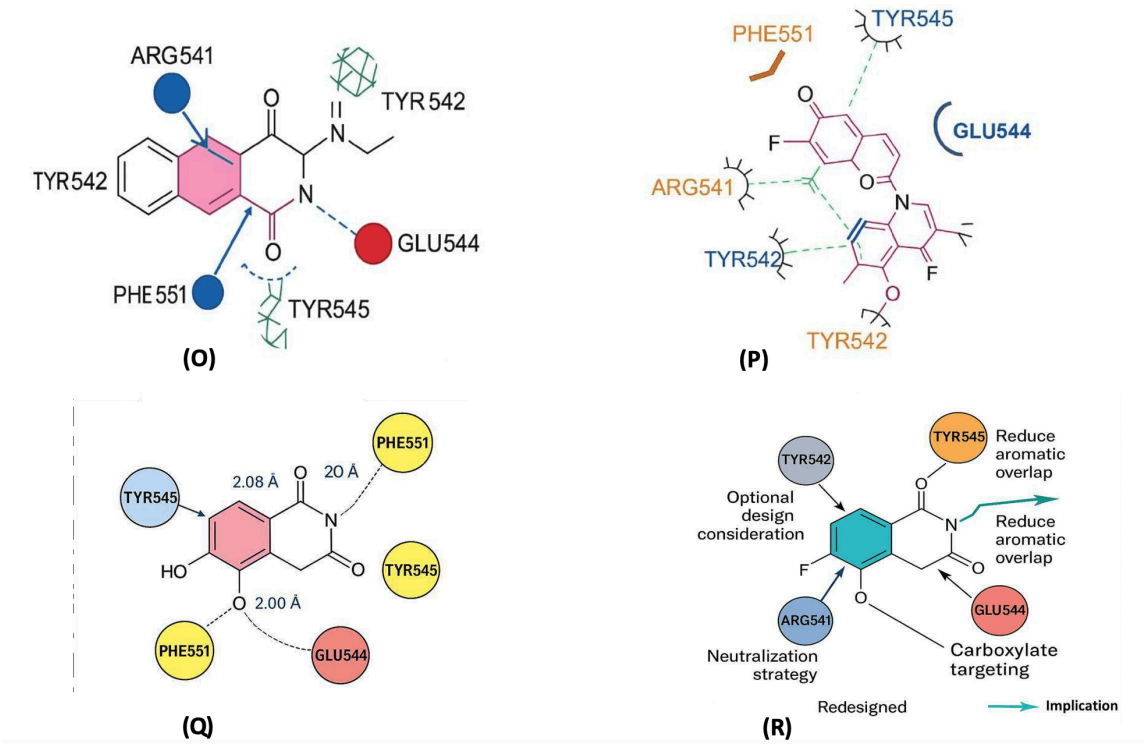

Figure 6. **(A)** Neural network–predicted target probability scores (DeepChem), showing interaction with neuroprotective proteins (e.g., GABA-A, CACNA1C). **(B)** 3D schematic structure of before modified structure, showing redesigned ligand embedded within the binding pocket showing interactions. **(C)** in ribbon cartoon structure of before modified structure showing residues interactions. **(D)** Zoomed-In View of Moxifloxacin Binding within the hERG Channel Hydrophobic Pocket. **(E)** Binding Pose of a Redesigned Fluoroquinolone within the hERG Channel Pocket. **(F)** Zoom-out view after modification structure showing hydrophobicity interaction network. **(G)** Zoom-in view after modification structure measuring the distance of residues. **(H)** Zoom- out view after modification structure showing hydrogen and pi-pi interaction network. **(I)** Zoom-in view interaction network. **(J)** Zoom-out view after modification structure showing salt bridges. **(K)** 2D Leview image of structure therapeutic repositioning of this molecule as a neuroprotective antibacterial agent. **(L)** 2D image of redesigned structure visualization using Ligplot. **(M)** 2D image of our redesigned structure using tools pose view for panel (M) and MOE for panel **(N)** to generate images. **(0)** 2D interaction map - strategic reduction of toxic interactions. **(P)** Confirmation of interactions-MOE/Ligplot view. **(Q)** 2D schematic POSEView interaction map. **(R)** Structure-Guided Redesign Strategy of Fluoroquinolone Targeting Key Residues in the hERG Binding Site.

doi.org/10.32388/TO3H6G

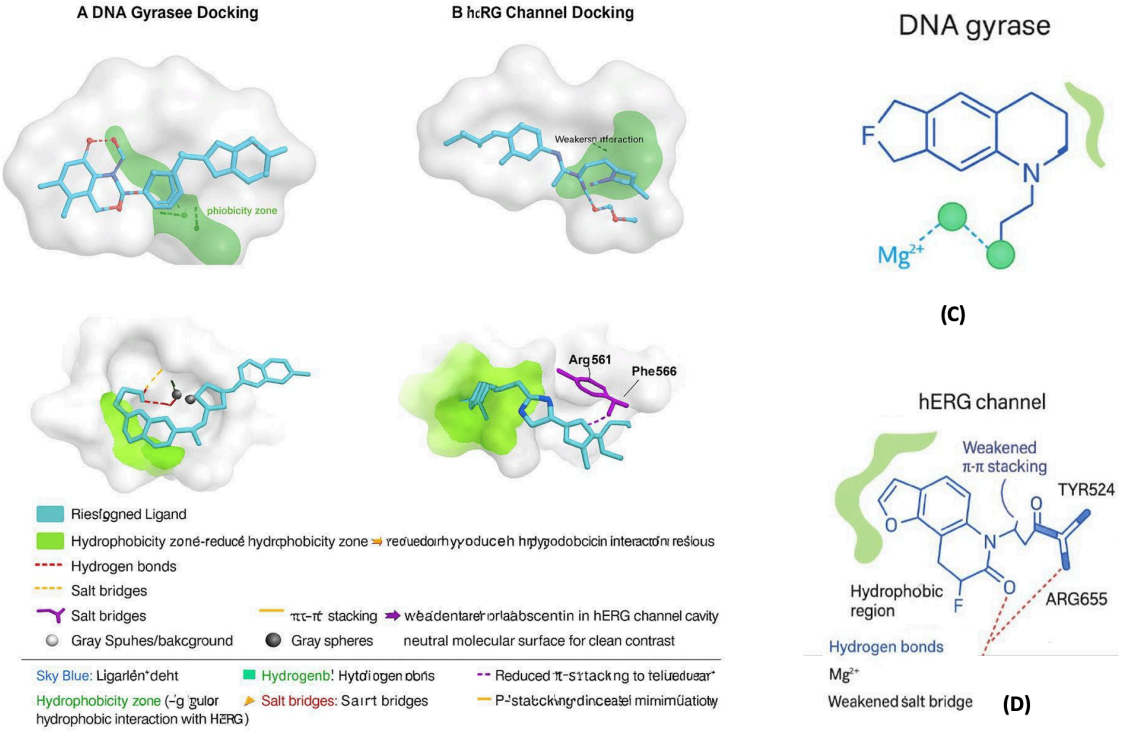

Figure 7. (A) 3D Binding interaction of the redesigned ligand (sky blue) with bacterial DNA gyrase, showing preservedantibacterial activitythrough key hydrogenbonds (red dashed lines)and Mg^{2+} coordination (gray spheres). Criticalresidues including Asp437, Ser84, and Glu58 form stable hydrogen bonding and bidentate interactions, supporting the ligand's functionality. **(B)** 3D Binding pose of the same ligand within the hERG potassium channel, illustrating attenuated cardiotoxic potential. The redesigned structure exhibits weakened $\pi-\pi$ stacking with Tyr652 and Phe656 (purple dashed lines), andabsence of salt bridges with Arg541 and Glu544 (yellow dashed lines). The hydrophobic region (green highlight) shows reduced interaction intensity, supporting reduced channel affinity. **(C)** 2D DNA Gyrase Docking): Shows retention of essential hydrogen bonding and Mg^{2+} coordination by redesigned ligand, ensuring preserved antibacterial action. Key residues involved include Asp437, Ser84, Glu58, and coordinated Mg^{2+} ions, forming strong H-bonds and bidentate interactions. **(D)** (hERG ChannelDocking): Redesigned ligand demonstrates reduced$\pi-\pi$ stacking with Tyr652 and Phe656, and absent salt bridges with Arg541 and Glu544, indicating attenuated binding affinity and minimized cardiotoxicity. Hydrophobic region marked in green shows weaker interaction within the channel cavity.

doi.org/10.32388/TO3H6G

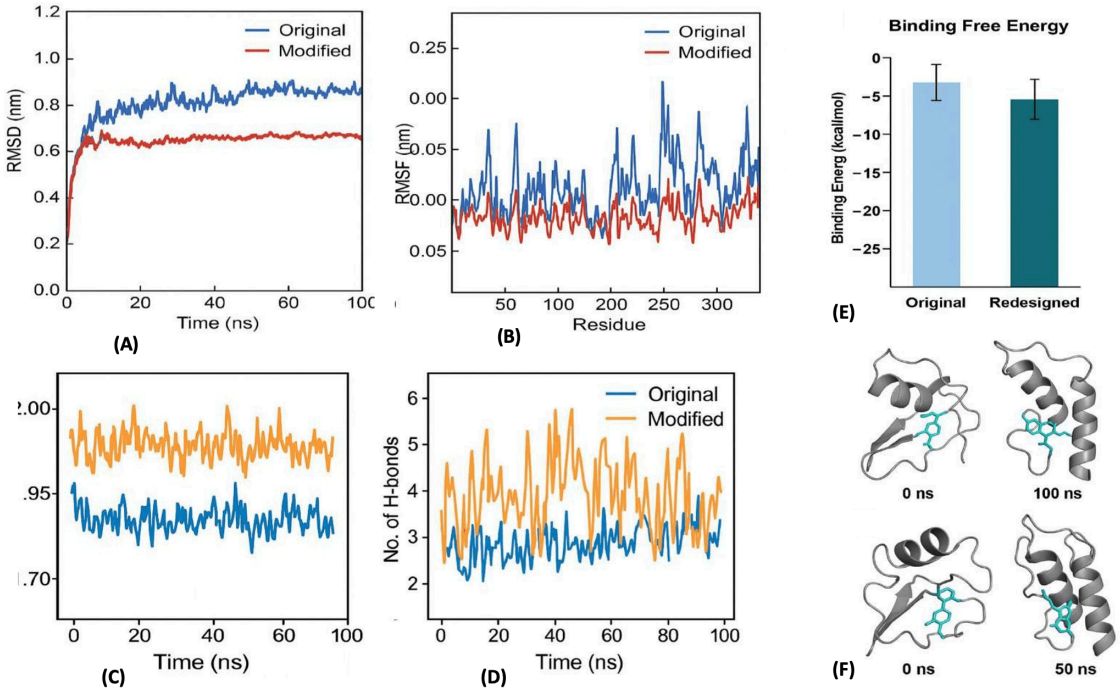

Figure 8. Comparative Molecular Dynamics (MD) simulation of the original and modified fluoroquinolone bound to the target protein. **(A)** Root Mean Square Deviation (RMSD) of the protein–ligand complexes over 100 ns, demonstrating improved structural stability in the modified derivative. **(B)** Root Mean Square Fluctuation (RMSF) per-residue, indicating local flexibility changes due to ligand binding. **(C)** Radius of gyration (Rg) plot reveals differences in protein compactness during simulation.**(D)** Hydrogen bond occupancy vs. time shows increased interaction persistence in the modified complex. **(E)** Binding free energy estimation (MM/PBSA or MM/GBSA) confirms enhanced affinity of the redesigned molecule. **(F)** Structural snapshots captured at 0 ns, 50 ns, and 100 ns highlighting conformational transitions in the binding site and global protein architecture.

Statements and Declarations

Acknowledgments

The authors gratefully acknowledge the use of institutional high-performance computing (HPC) resources provided by the computer-aided drug discovery (CADD) Core and support from the Texas Advanced Computing Center (TACC), which enabled molecular docking, molecular dynamics simulations, and MM-PBSA free energy calculations. AI-based target deconvolution and survival risk modeling were supported by open-access platforms including DeepChem, SwissTargetPrediction, and SHAP. The schematic illustrations were created using BioRender.com. The authors also recognize the critical contributions of SwissADME, ProTox-II, and PLIP for in silico pharmacokinetic, toxicity, and interaction profiling.

doi.org/10.32388/TO3H6G

Conflicts of interest

The authors declare no competing financial interests.

Funding

This research did not receive any specific grant from funding agencies in the public, commercial, or not-for-profit sectors.

Data and Materials

All data necessary to support the findings of this study are available within the manuscript and/or the Supplementary Materials. Additional datasets or analysis files related to this work may be obtained from the corresponding author upon reasonable request.

References

1. ^*Rodrigues CF, Silva F (2025). "The Rise, Fall, and Rethink of (Fluoro) Quinolones: A Quick Rundown." Pathogens.* ***14****(6):525. doi:10.3390/pathogens14060525.*
2. ^*Kherroubi L, Bacon J, Rahman KM (2024). "Navigating Fluoroquinolone Resistance in Gram-Negative Bacteria: A Comprehensive Evaluation." JAC Antimicrob Resist.* ***6****(4):dlae127. doi:10.1093/jacamr/dlae127.*
3. ^*Collins JA, Osheroff N (2024). "Gyrase and Topoisomerase IV: Recycling Old Targets for New Antibacterials to Combat Fluoroquinolone Resistance." ACS Infect Dis.* ***10****(4):1097–1115. doi:10.1021/acsinfecdis.4c00128.*
4. ^*Furutani K (2023). "Facilitation of hERG Activation by Its Blocker: A Mechanism to Reduce Drug-Induced Proarrhythmic Risk." Int J Mol Sci.* ***24****(22):16261. doi:10.3390/ijms242216261.*
5. ^*Zhao Y, Inayat S, Dikin DA, Singer JH, Ruoff RS, Troy JB (2014). "Patch Clamp Electrophysiology: Principle and Applications." J Vis Exp. (87):e5202. doi:10.3791/5202.*
6. ^*Gadhave DG, et al. (2024). "Neurodegenerative Disorders: Mechanisms of Degeneration and Therapeutic Approaches with Their Clinical Relevance." Ageing Res Rev. 102357. doi:10.1016/j.arr.2024.102357.*
7. ^*Jiang C, Chen Y, Sun T (2025). "From the Gut to the Brain: Mechanisms and Clinical Applications of γ-Aminobutyric Acid (GABA) on the Treatment of Anxiety and Insomnia." Front Neurosci.* ***19****:1570173. doi:10.3389/fnins.2025.1570173.*
8. ^*El-Saghier AM, Abosella L, Hassan A, Elakesh EO, Bräse S, Abuo-Rahma GE-DA, Aziz HA (2025). "Design, Synthesis, and In Silico Studies of New Norfloxacin Analogues with Broad-Spectrum Antibacterial Activity Via Topoisomerase II Inhibition." Pharmaceuticals.* ***18****(4):545. doi:10.3390/ph18040545.*

9. ^a ^b ^cEl-mrabet A, Haoudi A, Kandri-Rodi Y, Mazzah A (2025). "An Overview of Quinolones as Potential Drugs: Synthesis, Reactivity and Biological Activities." Organics. **6**:16.
10. ^Comajuncosa-Creus A, Jorba G, Barril X, et al. (2024). "Comprehensive Detection and Characterization of Human Druggable Pockets Through Binding Site Descriptors." Nat Commun. **15**:7917. doi:10.1038/s41467-024-52146-3.
11. ^Czyżnikowska Ż, Mysłek M, Marciniak A, et al. (2025). "In Silico Approach to Design of New Multi-Targeted Inhibitors Based on Quinoline Ring with Potential Anticancer Properties." Int J Mol Sci. **26**(10):4620. doi:10.3390/ijms26104620.
12. ^a ^bAbbas MKG, Rassam A, Karamshahi F, Abunora R, Abouseada M (2024). "[Title Not Available]." ChemBioChem. doi:10.1002/cbic.202300816.
13. ^Wan Z, Sun X, Li Y, et al. (2025). "Applications of Artificial Intelligence in Drug Repurposing." Adv Sci. doi:10.1002/advs.202411325.
14. ^Alisaac A (2025). "In Silico Analysis of Quorum Sensing Modulators: Insights Into Molecular Docking and Dynamics and Potential Therapeutic Applications." PLoS One. **20**(6):e0325830. doi:10.1371/journal.pone.0325830.
15. ^Ocana A, Pandiella A, Privat C, et al. (2025). "Integrating Artificial Intelligence in Drug Discovery and Early Drug Development: A Transformative Approach." Biomark Res. **13**:45. doi:10.1186/s40364-025-00758-2.
16. ^Trezza A, Visibelli A, Roncaglia B, et al. (2025). "Unveiling Dynamic Hotspots in Protein–Ligand Binding: Accelerating Target and Drug Discovery Approaches." Int J Mol Sci. **26**(9):3971. doi:10.3390/ijms26093971.
17. ^Cheng Y, Yu TT, Olzomer EM, et al. (2025). "Design, Synthesis, and Biological Evaluation of Naphthoquinone Salts as Anticancer Agents." Molecules. **30**(9):1938. doi:10.3390/molecules30091938.
18. ^Phuagkhaopong S, Sukwattanasombat J, Suknuntha K, et al. (2025). "Anti-Inflammatory Effects of Moxifloxacin and Levofloxacin on Cadmium-Activated Human Astrocytes: Inhibition of Proinflammatory Cytokine Release, TLR4/STAT3, and ERK/NF-κB Signaling Pathway." PLoS One. **20**(1):e0317281. doi:10.1371/journal.pone.0317281.
19. ^a ^b ^cHryhoriv H, Kovalenko SM, Georgiyants M, et al. (2023). "A Comprehensive Review on Chemical Synthesis and Chemotherapeutic Potential of 3-Heteroaryl Fluoroquinolone Hybrids." Antibiotics. **12**(3):625. doi:10.3390/antibiotics12030625.
20. ^Wan Z, Sun X, Li Y, Chu T, Hao X, Cao Y, Zhang P (2025). "Applications of Artificial Intelligence in Drug Repurposing." Adv Sci (Weinh). **12**(14):e2411325. doi:10.1002/advs.202411325.
21. ^a ^bBarberán J, de la Cuerda A, Tejeda González MI, López Aparicio A, Monfort Vinuesa C, Ramos Sánchez A, Barberán LC (2024). "Safety of Fluoroquinolones." Rev Esp Quimioter. **37**(2):127–133. doi:10.37201/req/143.2023.
22. ^Reinhardt T, El Harraoui Y, Rothemann A, et al. (2025). "Chemical Proteomics Reveals Human Off-Targets of Fluoroquinolone-Induced Mitochondrial Toxicity." Angew Chem Int Ed Engl. doi:10.1002/anie.202421424.

23. ^Li VOK, Han Y, Kaistha T, et al. (2025). "DeepDrug as an Expert Guided and AI-Driven Drug Repurposing Methodology for Selecting the Lead Combination of Drugs for Alzheimer's Disease." Sci Rep. **15**:2093. doi:10.1038/s41598-025-85947-7.

24. ^Kim J, Shin SA, Lee CS, Chung HJ (2023). "An Improved In Vitro Blood-Brain Barrier Model for the Evaluation of Drug Permeability Using Transwell With Shear Stress." Pharmaceutics. **16**(1):48. doi:10.3390/pharmaceutics16010048.

25. ^Reaven NL, Yang M, Schwartz EJ, Hu X, Funk SE, Caban A, et al. (2023). "Use of Artificial Intelligence for Drug Development and Clinical Trial Design: A Translational Perspective." Clin Transl Sci. **16**(6):1173–82. doi:10.1111/cts.13103.

26. ^Pantelidis P, Dilaveris P, Ruipérez-Campillo S, et al. (2025). "Hearts, Data, and Artificial Intelligence Wizardry: From Imitation to Innovation in Cardiovascular Care." Biomedicines. **13**(5):1019. doi:10.3390/biomedicines13051019.

27. ^Iftikhar H (2025). "AI-Driven Pharmacovigilance and Molecular Profiling of Fluoroquinolone-Associated Cardiotoxicity in the UAE: A Geospatial and Machine Learning Analysis With Structural Modification Strategies (2018–2023)." bioRxiv [Preprint]. May 5. doi:10.1101/2025.05.10.25327319.

28. ^Vittorio S, Lunghini F, Pedretti A, Vistoli G, Beccari AR (2023). "Ensemble of Structure and Ligand-Based Classification Models for hERG Liability Profiling." Front Pharmacol. **14**:1148670. doi:10.3389/fphar.2023.1148670.

29. ^Negami T, Terada T (2023). "Calculations of the Binding Free Energies of the Comprehensive In Vitro Proarrhythmia Assay (CiPA) Reference Drugs to Cardiac Ion Channels." Biophys Physicobiol. **20**(2):e200016. doi:10.2142/biophysico.bppb-v20.0016.

Supplementary data: available at https://doi.org/10.32388/TO3H6G

Declarations

Funding: No specific funding was received for this work.

Potential competing interests: No potential competing interests to declare.